Horizon 2020 Programme

METIS

Research and Innovation Action (RIA)

This project has received funding from the European Union's Horizon 2020 research and innovation programme under grant agreement No 945121

Start date : 2020-09-01 Duration : 48 Months

Application of Bayesian updating techniques to the seismic fragility of nuclear structures, case of SMART2013 mockup

Authors : Dr. David BOUHJITI (IRSN), Try MENG, David BOUHJITI, Benjamin RICHARD

METIS - Contract Number: 945121

Project officer: Katerina PTACKOVA

Document title	Application of Bayesian updating techniques to the seismic fragility of nuclear structures, case of SMART2013 mockup
Author(s)	Dr. David BOUHJITI, Try MENG, David BOUHJITI, Benjamin RICHARD
Number of pages	52
Document type	Deliverable
Work Package	WP6
Document number	D6.6
Issued by	IRSN
Date of completion	2024-04-12 14:25:44
Dissemination level	Public

Summary

The deliverable 6.6 (D6.6) is one of the tasks within the work package 6 (WP6) dealing with beyond design assessment and fragility analysis. The D6.6 focuses on the application of Bayesian updating techniques to reduce the uncertainties on the fragility curves. In this report, the Bayesian technique is applied to update the inputs characterizing the mechanical behaviour of structural elements made from reinforced concrete and subjected to seismic input ground motion. The main sources of uncertainties come either from the so-called aleatory uncertainty (associated to the intrinsic random nature of some specific phenomena) or from epistemic uncertainties (associated to the limited knowledge we may have given a specific phenomenon). The objective here is to develop a methodology based on the Bayesian approach using the available measurements to limit the effect of such uncertainties on the model?s predictive capacity. This includes updating the current state of parameters for the constitutive law of the material and of boundary conditions to get what one observes or at least approach it to the best. With these new inputs, one can launch new numerical simulations with a realistic resulting mechanical state with, hopefully, reduced epistemic uncertainties. In fact, the Bayesian updating technique is popular and widely used in various domains. One of the applications of interest in this work is to estimate the fragility curve by updating the structural capacity and to assess the seismic margins at low and high PGAs. In the framework of METIS project, for the sake of illustration, the Bayesian approach is applied for the SMART2013 mock-up using the linear elastic equivalent method. In this work, the consideration of Bayesian updating using nonlinear modelling is beyond the present scope. However, we mention that the global methodology remains the same and that it is expected that the computational time will be higher compared to linear equivalent analysis.

Approval

Date	By
2024-04-17 15:06:50	Mrs. Shadi FATHABADI (TUK)
2024-04-17 16:58:56	Dr. Irmela ZENTNER (EDF)

METIS

Seismic Risk Assessment
for Nuclear Safety

Research & Innovation Action

NFRP-2019-2020

Application of Bayesian updating techniques to the seismic fragility of nuclear structures – case of SMART2013 mock-up

Deliverable D6.6

Version N°003

Author: Try MENG

Radioprotection and Nuclear Safety Institute (IRSN)
Structural Performance Modeling and Analysis Laboratory (LMAPS)

Disclaimer

The content of this deliverable reflects only the author's view. The European Commission is not responsible for any use that may be made of the information it contains.

Document Information

Grant agreement	945121
Project title	Methods And Tools Innovations For Seismic Risk Assessment
Project acronym	METIS
Project coordinator	Dr. Irmela Zentner, EDF
Project duration	1st September 2020 – 31st August 2024 (48 months)
Related work package	WP 6- Beyond design and fragility analysis
Related task(s)	Task 6.6 – Application of Bayesian updating techniques
Lead organisation	IRSN
Contributing partner(s)	
Due date	December 31st 2023
Submission date	
Dissemination level	Public

History

Version	Submitted by	Reviewed by	Date	Comments
N°001	Try MENG, IRSN	David BOUHJITI, IRSN Benjamin RICHARD, IRSN	22/12/2023	-
N°002	David BOUHJITI, IRSN	Shadi FATHABADI, RPTU Irmela ZENTNER, EDF R&D	06/02/2024	Updated list of figures Updated Fig. 25, 34 and 36 New appendix 10.1
N°003	David BOUHJITI, IRSN	Claudia Redenbach, RPTU	18/03/2024	Correction of few notations Correction of the normalization constant in 4.2.2

Table of Contents

1. Introduction 10

2. Overview of the experimental campaign SMART2013 11

2.1. Geometry of the mock-up 11
2.2. Shaking table 12
2.3. Material properties 12
2.4. Seismic loading 13
2.5. Available measurement 13

3. Numerical simulation 15

3.1. Numerical mock-up 15
3.2. Damping model 15
3.3. Application of the seismic loads 16
3.4. Boundary conditions 16
3.5. Material properties 16
3.6. Results of blind calculations 16
3.6.1. Eigenfrequencies 17
3.6.2. Acceleration response spectra 17

4. Theory of metamodeling and Bayesian updating 19

4.1. Polynomial Chaos Expansion 19
4.2. MCMC Bayesian updating 19
4.2.1. General framework of probabilistic models 19
4.2.2. Bayesian inverse problem and MCMC algorithms 20

5. Global Bayesian updating strategy on SMART mock-up 21

6. Application to elastic and nonlinear cases 22

6.1. Elastic runs #7 #9 #11 22
6.1.1. Updating of eigenfrequencies 22
6.1.2. Updating of acceleration spectra 24
6.2. Nonlinear run #19 27
6.2.1. Updating Eigenfrequencies 27
6.2.2. Updating acceleration spectra 29
6.3. Overview of all results 31

7. Updating of fragility curves 33

7.1. Principle of fragility computation 33
7.2. Fragility curve based on spectral accelerations 33
7.3. Fragility curve based on inter-story drift 34

8. Conclusion 36

9. Applicability of the approach at an industrial scale 36

10. Bibliography 37

11. Appendix 38

11.1. Detailed example for PCE application 38
11.1.1. Metamodel for acceleration response spectra (run 9) 38
11.1.2. Metamodel for inter-storey drift (run 9) 41
11.2. Run #9 43
11.2.1. Metamodel for the 2nd Bayesian (ξ_1; ξ_2 ➔ S_a) 43
11.2.2. Updated damping ratios 43
11.2.3. Verification 43
11.3. Run #11 44
11.3.1. Metamodel for the 2nd Bayesian (ξ_1; ξ_2 ➔ S_a) 44
11.3.2. Updated damping ratios 44
11.3.3. Verification 45
11.4. Run #15 46
11.4.1. Updated Young's modulus 46
11.4.2. Metamodel for the 2nd Bayesian (ξ_1; ξ_2 ➔ S_a) 48
11.4.3. Updated damping ratios 48
11.4.4. Verification 48
11.5. Run #17 49
11.5.1. Updated Young's modulus 49
11.5.2. Metamodel for the 2nd Bayesian (ξ_1; ξ_2 ➔ S_a) 51
11.5.3. Updated damping ratios 52
11.5.4. Verification 52

List of figures

Figure 1: View of the full-scale building (in blue) and the reactor building (in grey) 11

Figure 2: SMART mock-up on shaking table (AZALEE/CEA) 11

Figure 3: experimentally boundary condition 12

Figure 4: shaking table (AZALEE) 12

Figure 5: Modal deformations (elastic case) 14

Figure 6: position of measurement points 14

Figure 7: numerical finite elements model of the SMART2013 mock-up (including the shaking table) 15

Figure 8: damping based on Rayleigh model 15

Figure 9: recorded acceleration at the center of shaking table (run #19) 16

Figure 10: acceleration response spectra (run #7) 18
Figure 11: acceleration response spectra (run #19)..... 18
Figure 12: methodology of Bayesian on SMART mock-up..... 21
Figure 13: scope of Bayesian updating 21
Figure 14: configuration of 1st Bayesian updating step..... 22
Figure 15: uniform distribution..... 23
Figure 16: three modes of eigenfrequencies 23
Figure 17: comparison of metamodel with numerical simulation results 23
Figure 18: configuration of elastic runs..... 23
Figure 19: prior/posterior of Young's modulus and estimation of eigenfrequencies . 24
Figure 20: comparison of metamodel vs. numerical simulation results (for run #7) 25
Figure 21: prior and posterior distribution of damping ratios, ξ_1 ; ξ_2 (run #7)..... 26
Figure 22: acceleration response spectra at control point D (run #7)..... 26
Figure 23: acceleration response spectra at point B (run #7) 27
Figure 24: prior/posterior of Young's modulus distribution on wall (V_12)..... 28
Figure 25: prior/posterior of Young's modulus distribution on walls and foundation 28
Figure 26: prior/posterior of Young's modulus distribution on the slabs 29
Figure 27: comparison of Metamodel with numerical simulation run #19 30
Figure 28: prior and posterior distribution of damping ratios, ξ_1 ; ξ_2 (run #19)..... 30
Figure 29: acceleration response spectra at control point D (run #19)..... 31
Figure 30: acceleration response spectra at point B (run #19) 31
Figure 31: Effective Young's modulus reduction factor (left: wall; right: slab)..... 32
Figure 32: updated damping ratios for different runs..... 32
Figure 33 : computation of fragility curve method 33
Figure 34: fitted linear model: spectral acceleration vs. PGA (left) prior (right) posterior..... 34
Figure 35: fragility curve for spectral accelerations 34
Figure 36: fitted linear model : drift vs. PGA (left) prior (right) posterior..... 35
Figure 37: fragility curves for inter-story drift with a threshold at (left:4‰ ; right:6‰) 35
Figure 38: random values of damping ratios 38
Figure 39: output as acceleration response spectra 39

Figure 40: output as inter-storey drift at point D 41
Figure 41: comparison of metamodel response vs. computed values using Cast3m 42
Figure 42: comparison of Metamodel with numerical simulation (run #9) 43
Figure 43: prior/posterior damping ratios distribution 43
Figure 44: comparison of acceleration response spectra (5%) at point D 43
Figure 45: comparison of acceleration response spectra (5%) at point B 44
Figure 46: comparison of Metamodel with numerical simulation (run #11)..... 44
Figure 47: prior/posterior damping ratios distribution 44
Figure 48: comparison of acceleration response spectra (5%) at point D 45
Figure 49: comparison of acceleration response spectra (5%) at point B 45
Figure 50: prior/posterior Young's modulus distribution (wall : V_{12}) 46
Figure 51: prior/posterior Young's modulus distribution (wall + foundation)..... 46
Figure 52: prior/posterior Young's modulus distribution (slab)..... 47
Figure 53: comparison of Metamodel with numerical simulation (run #15)..... 48
Figure 54: prior/posterior damping ratios distribution 48
Figure 55: comparison of acceleration response spectra (5%) at point D 48
Figure 56: comparison of acceleration response spectra (5%) at point B 49
Figure 57: prior/posterior Young's modulus distribution (wall : V_{12}) 49
Figure 58: prior/posterior Young's modulus distribution (wall + foundation)..... 50
Figure 59: prior/posterior Young's modulus distribution (slab)..... 50
Figure 60: comparison of Metamodel with numerical simulation (run #17)..... 51
Figure 61: prior/posterior damping ratios distribution 52
Figure 62: comparison of acceleration response spectra (5%) at point D 52
Figure 63: comparison of acceleration response spectra (5%) at point B 52

List of tables

Table 1: Dimension of structural elements 11
Table 2: material properties of concrete 13
Table 3: material properties of steel rebar 13
Table 4: peak ground acceleration measured on shaking table 13
Table 5: measured eigenfrequencies 14
Table 6: statistic parameters for concrete properties 16
Table 7: comparison of eigenfrequencies between num vs. exp 17
Table 8: Young's modulus proposed in numerical design plan 22
Table 9: prior and posterior properties of Young's modulus 24
Table 10: damping ratio proposed in numerical design plan 25
Table 11: prior and posterior properties of damping ratios 25
Table 12: prior and posterior of Young's modulus 29
Table 13: prior and posterior of damping ratios (runs #15; #17; #19) 30
Table 14: prior and posterior error functions: spectral acceleration vs. PGA 34
Table 15: prior and posterior error functions: drift vs. PGA 35
Table 16: illustration the form of polynomials (Marelli, 2022) 39
Table 17: coefficients of polynomial function (spectral acceleration #run9) 40
Table 18: coefficients of polynomial function (drift #run9) 42
Table 19: prior and posterior of Young's modulus 47
Table 20: prior and posterior of Young's modulus 51

Abbreviations and Acronyms

Acronym	Description
WP	Work Package
MCMC	Markov Chain Monte Carlo
PCE	Polynomial chaos expansion
ξ	Damping ratio
E_c	Concrete Young's modulus
S_a	Acceleration response spectra (5% damping)
δ	Drift
f_1; f_2; f_3	First eigenfrequencies of three main modes

Summary

The main objective of this task is to develop an operational methodology of Bayesian updating to be applied to the seismic behaviour of nuclear buildings. The case of application is the SMART2013 mock-up. The Bayesian updating is an efficient tool to improve the estimations of the structural responses (acceleration response spectra and displacements amongst others) by updating a limited number of influential inputs based on available measurements and observations. In this work, the Bayesian updating is applied using a dynamic model that is based on the principle of elastic equivalent analysis. So, the reinforced concrete behaviour is considered as being elastic and the seismic induced damage is modelled by reducing the Young's modulus of cracked elements and by increasing the global reduced damping ratio of the structure.

Obviously, the Young's modulus reduction and reduced damping ratio amplification depend on the amplitude of the seismic load; here characterized by its Peak Ground Acceleration (PGA with values between 0.5 and 5 times the design level). As the Bayesian updating might require a large number of iterations and calculations depending on the gap between the prior and posterior estimates, the usage of equivalent linear based models might not suffice to cope with the curse of dimensionality. Therefore, we also consider the development of substitution models (or metamodels) for each Engineering Demand Parameter (EDP) of interest (here it is the case of spectral accelerations and drift values).

The application of Bayesian updating to those two EDPs leads to a general improvement of the model's capacity to describe the overall behaviour of the structure under seismic loads. Once the new posterior distributions of our inputs (Young's modulus and damping ratio) are known, the metamodels are used again to compute fragility curves considering illustrative failure threshold for the spectral accelerations and for the drift values. The quantification of these fragility curves is based on the principle of statistical regression of each quantity (EDP) as a function of the PGA to which we add an error function representative of the distribution of gaps between the fitted model and the computed values. That error function is supposed to be centred and follows a normal distribution with a given standard deviation. As the updating is applied, and in addition for the general improvement of the model's accuracy, we also observe that the confidence level width between 5% and 95% is considerably reduced with respect to the one obtained in case of the prior estimations.

Keywords

Bayesian updating; metamodeling; Young's modulus; damping ratio; fragility curve; acceleration response spectra; drift.

1. Introduction

The deliverable 6.6 (D6.6) is one of the tasks within the work package 6 (WP6) dealing with beyond design assessment and fragility analysis. The D6.6 focuses on the application of Bayesian updating techniques to reduce the uncertainties on the fragility curves. In this report, the Bayesian technique is applied to update the inputs characterizing the mechanical behaviour of structural elements made from reinforced concrete and subjected to seismic input ground motion. The main sources of uncertainties come either from the so-called aleatory uncertainty (associated to the intrinsic random nature of some specific phenomena) or from epistemic uncertainties (associated to the limited knowledge we may have given a specific phenomenon). The objective here is to develop a methodology based on the Bayesian approach using the available measurements to limit the effect of such uncertainties on the model's predictive capacity. This includes updating the current state of parameters for the constitutive law of the material and of boundary conditions to get what one observes or at least approach it to the best. With these new inputs, one can launch new numerical simulations with a realistic resulting mechanical state with, hopefully, reduced epistemic uncertainties.

In fact, the Bayesian updating technique is popular and widely used in various domains (see for example the work of (Richard B. A., 2012; Rossat D. B.-P., 2022; Rossat D. B.-M., 2021; Tekeste, 2022; Wang, 2018). One of the applications of interest in this work is to estimate the fragility curve by updating the structural capacity ($\tilde{A}_m$); to assess the seismic margins at low and high PGAs. In the framework of METIS project, for the sake of illustration, the Bayesian approach is applied for the SMART2013 mock-up (Belletti, 2017; Richard B. C.-E., 2016; Richard B. M., 2015) using the linear elastic equivalent method. The aim, through updating, is to:

- in a first time, to update the effective properties of cracked structural elements (Young's modulus and damping ratio) based on the recorded and experimental eigenfrequencies; acceleration and observed cracking patterns;

- in a second time, to update the fragility curves using the updated inputs variables.

In this work, the consideration of Bayesian updating using nonlinear modelling is beyond the present scope. However, we mention that the global methodology remains the same and that it might take more computational time as the number of random variables increases including for instance the tensile strength, the fracture energy and the hysteretic damping ratio.

2. Overview of the experimental campaign SMART2013

The SMART2013 experimental campaign is based on a ¼ scaled mock-up of a building that is attached to the reactor building (Figure 1) with a strong sensitivity to the torsional behavior under seismic loads. This mock-up is bolted to the shaking table through 34 thread stalks at the foundation level (Figure 2). The mock-up consists of walls; slabs; beams; foundation and column to assure the stability during the tests. Masses are added to each floor (around 11 tons) to meet the scaling effects criteria. As for the seismic loads, three seismic sequences are considered: the design level (0.2g), Northridge main-shock (1.78g) and Northridge after-shock (0.37g). These loads are applied in an increasing way through several runs. During each run, the mock-up is monitored to measure the displacements, the accelerations, crack openings, strains within concrete, uplift at the foundation level.

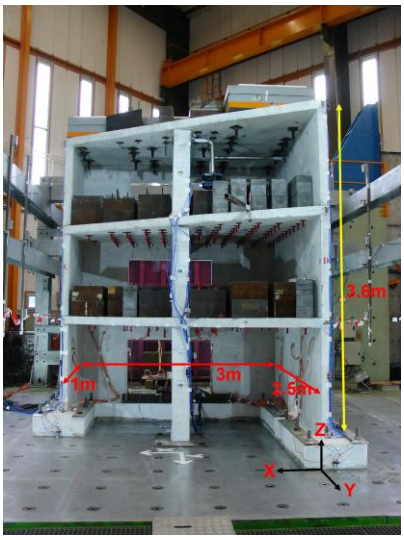

Figure 2: SMART mock-up on shaking table (AZALEE/CEA)

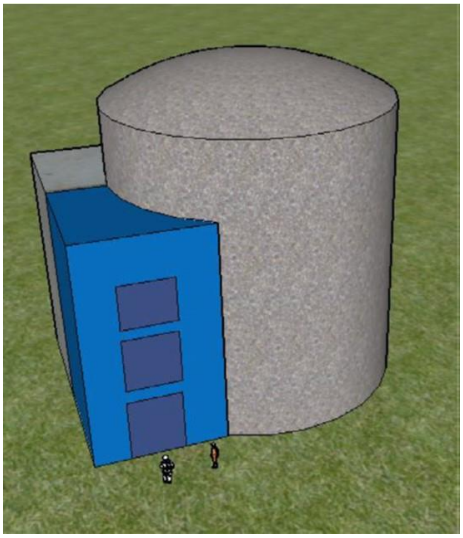

Figure 1: View of the full-scale building (in blue) and the reactor building (in grey)

2.1. Geometry of the mock-up

The geometrical properties of structural elements in the mock-up are summed up in Table 1. The beams are located at the middle of the slabs, and the column ensures a stability function of the whole structure during the experiments. The dead weight of the mock-up is about 12 tons.

Description	Length (m)	Thickness (m)	Height (m)
Wall (01+02)	3	0.1	3.65
Wall 03	2.5		
Wall 04	1		
column	0.2	0.2	
beam	1.45	0.15	0.325
foundation	0.65	0.25	
	length (m)	thickness (m)	width (m)
slab	3	0.1	2.5

Table 1: Dimension of structural elements

2.2. Shaking table

The seismic tests were realized through the shaking table AZALEE installed at CEA (Figure 4). The shaking table is a 6x6m aluminium plate with a maximum capacity load of 100 tons. It is equipped with eight hydraulic actuators, 4 horizontal actuators at the sides and 4 vertical actuators at the bottom of the table. Each actuator can provide at maximum of 1 MN. The SMART mock-up is attached to the table through bolts crossing the foundation (Figure 4).

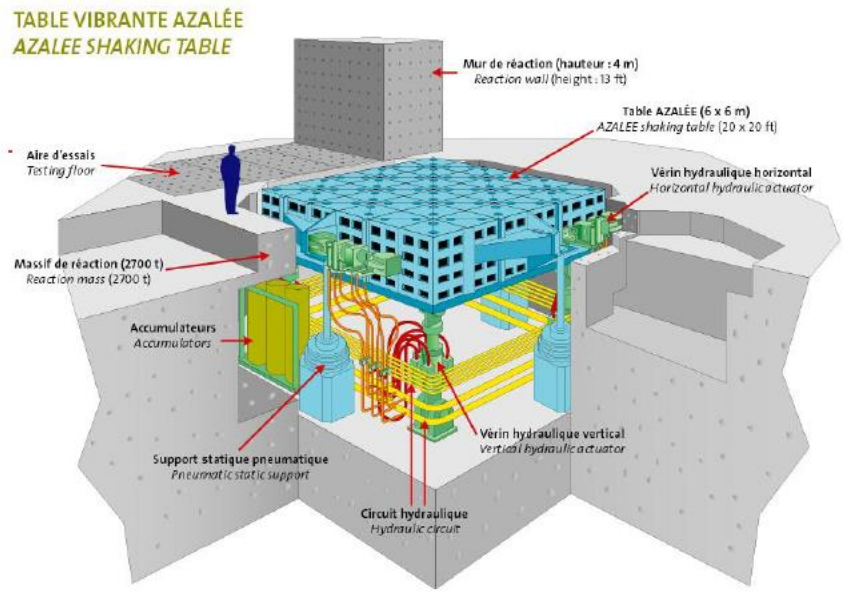

Figure 4: shaking table (AZALEE)

Figure 3: experimentally boundary condition

2.3. Material properties

- Concrete material

The mechanical properties of concrete elements are presented in Table 2: the fracture energy Gf, the tensile strength ft, the Young's modulus Ec, the Poisson's coefficient η. It should be reminded that those values are averaged from measurements of three specimens.

description	Gf (N/m)	ft (MPa)	Ec (MPa)	η
Foundation	135	4.14	25400	0.17
Wall (level 1)	136	3.9	28700	0.19
Floor (level 1)	133	3.74	28200	0.18
Wall (level 2)	132	3.78	25700	0.19
Floor (level 2)	113	3.32	24700	0.17
Wall (level 3)	123	3.57	29500	0.18
Floor (level 3)	135	3.9	24400	0.18

Table 2: material properties of concrete

- Steel material

The steel properties were measured on different diameters of the rebar. The yield stress and Young's modulus are summarized in Table 3.

diameter (mm)	fe (MPa)	fe/fy	Ea (GPa)
10 (ribbed)	500	1.14	202
8 (ribbed)	505	1.12	204
6 (ribbed)	528	1.1	207
4 (smooth)	665	1.06	202

Table 3: material properties of steel rebar

2.4. Seismic loading

In Table 4, the peak ground acceleration (PGA) effectively measured at the centre of the shaking table are presented for various runs. Two seismic sequences are assigned, they are the design level and Northridge main shock. The seismic intensity for each run is increased progressively.

# run	PGAx (g)	PGAy (g)	Description
7	0.13	0.13	Design level
9	0.21	0.24	
11	0.21	0.15	Northridge main shock
15	0.38	0.22	
17	0.56	0.39	
19	1.08	0.9	

Table 4: peak ground acceleration measured on shaking table

2.5. Available measurement

The recoded results include accelerations, displacements and cracking over time in addition to the eigenfrequencies and eigen modal deformations. In Figure 6, the control points are mostly located on the 4 corners of each floor and 2 points are at the floor level to monitor the vertical displacements. A measured point on the centre of the shaking table is recoded as well and is later used as the input

acceleration signal for the numerical simulation. In Table 5, the measured eigenfrequencies are provided. The drop of eigenfrequencies take place from run #15, that is also the run from which several cracking patterns are observed and evolve in the mock-up.

Run	f1 (Hz)	f2 (Hz)	f3 (Hz)
#7 ; #9 ; #11	6.1	7.8	16.5
#15	4.4	6.5	13
#17	4	5.7	12.7
#19	2.8	4.4	9

Table 5: measured eigenfrequencies

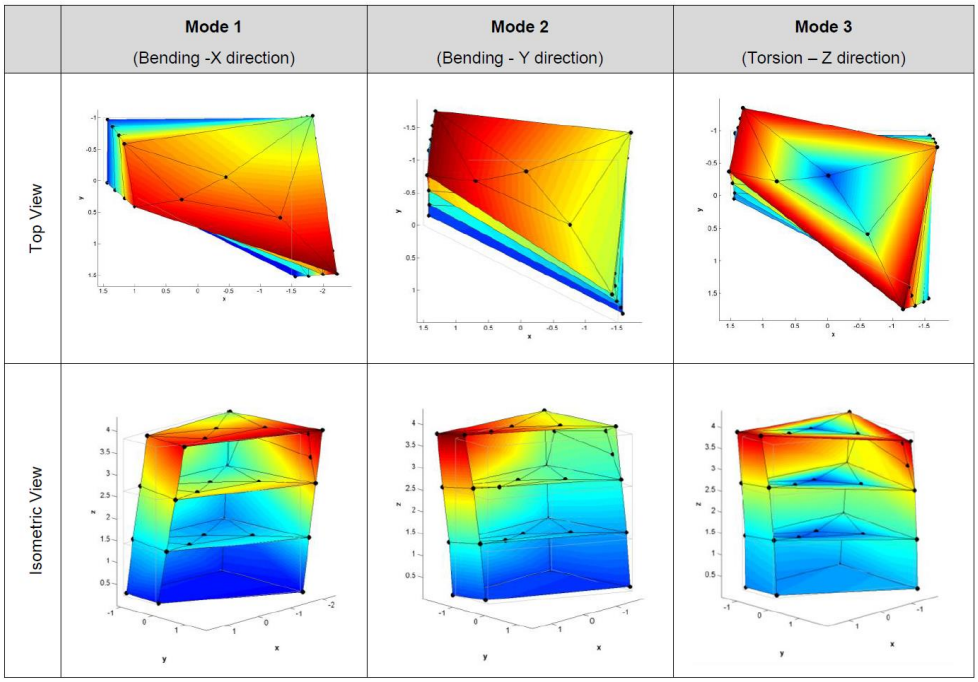

Figure 5: Modal deformations (elastic case)

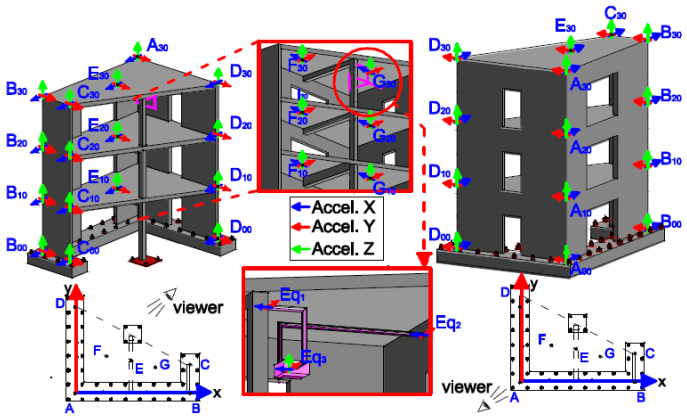

Figure 6: position of measurement points

3. Numerical simulation

3.1. Numerical mock-up

The numerical simulation is done using the Cast3m software (version 2021). As shown in Figure 7, the structural elements such as walls; floors and beams are modelled using multi-layered shell elements (5 layers for concrete). The foundation is modelled by the solid elements. The rebars are modelled using 4 additional layers (1 layer for each reinforcement direction). The mesh density is globally set at about 20 cm. The shaking table is also modelled by shell elements and is calibrated in order to obtain the relevant eigenfrequencies of the shaking table.

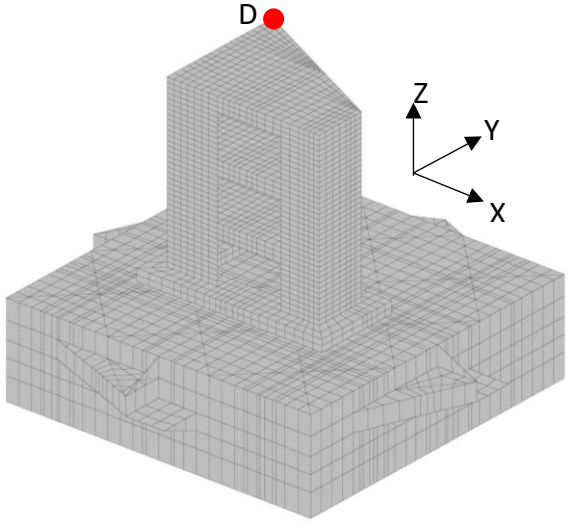

Figure 7: numerical finite elements model of the SMART2013 mock-up (including the shaking table)

3.2. Damping model

The damping of the structure is modelled through the Rayleigh model where the damping matric is a linear combination of the mass and stiffens matrix. Such model is well defined using two frequencies defining the range of interest (here we consider the first f1 and third f3 main eigenfrequencies) and a target damping value for each frequency. Based on experimental measurements, the damping ratios for these two frequencies are of 2.2% and 5.5% respectively (case of elastic behavior – no damage). This leads to the following evolution of damping with the frequency (Figure 8).

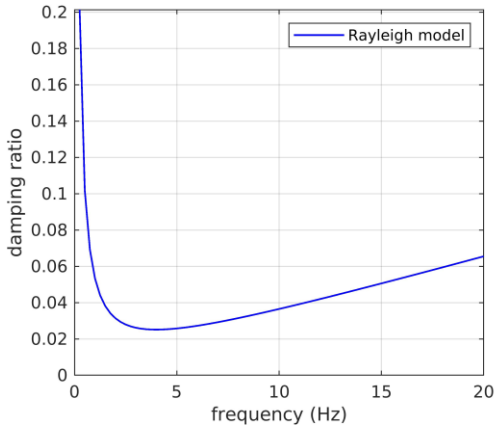

Figure 8: damping based on Rayleigh model

The calibration of the Rayleigh model is not obvious since both the frequencies and the damping values evolve with the damage state. The Bayesian updating is a good solution to better quantify the model's parameters based on available measurements.

3.3. Application of the seismic loads

The seismic loads are applied using force-controlled approach: the measured accelerations (X; Y; Z) at the centre of shaking table are multiplied by the weight distribution within the structure and the shaking table. An example of measured acceleration of run #19 is provided in Figure 9.

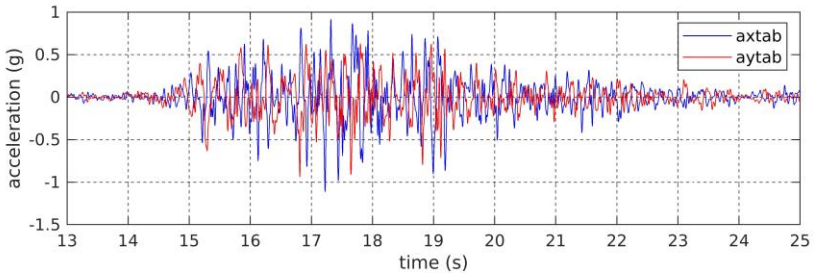

Figure 9: recorded acceleration at the center of shaking table (run #19)

3.4. Boundary conditions

The numerical boundary conditions are imposed at the position of the actuators of the shaking table. The vertical displacements are block at the 4 actuators on the bottom of the table. The displacements in X and Y are respectively blocked on the X and Y actuators.

As for the connection between the mock-up and the shaking table, the model does not include any bolts and the nodes of the foundation and of the shaking table are fully merged (perfect kinematic bond). The interaction between the table and the mock-up is modelled by modifying the Young's modulus value of the massive foundations in the model. Again, this is not easy to predict (stiffness of the shaking table – mock-up interaction), so the Bayesian updating is one efficient solution to improve the model's predictive capacity.

3.5. Material properties

As presented in Table 2, different concrete properties are introduced. Their average (avg) and standard deviation (std) values are shown in Table 6. It is seen that the coefficient of variation (cov=std/avg) are relatively small for the Poisson's coefficient (η). Thus, this parameter can be considered deterministic whereas the rest of inputs can be considered random and uncertain.

	f_c (MPa)	f_t (MPa)	E_c (MPa)	η	Gf (N/m)
Num	19	21	7	7	7
median	40.5	3.3	25700	0.18	133.6
mean	40	3.3	26657	0.18	130
std	3.93	0.44	2083	0.008	8.3
Cov(%)	9.8	13.3	7.8	4.5	6.4

Table 6: statistic parameters for concrete properties

3.6. Results of blind calculations

Before applying the Bayesian updating to the model, we run here blind calculations to quantify the gap between numerical and experimental results.

3.6.1. Eigenfrequencies

Runs #7 and #19 are experimentally considered as elastic (no cracking) and nonlinear (cracks observed) runs.

- for run #7, the blind simulation is exclusively based on the input parameters measured at the sample scale, including the concrete's Young's modulus and damping ratio as well.
- for run #19, the blind simulation is described by the hypothesis of equivalent elastic simulation where the Young's modulus of concrete's cracked elements are divided by 2 and the global damping ratio is set to 7%.

The comparison of global eigenfrequencies (f1,f2,f3) between the blind numerical simulations and experimental results is provided in Table 7. Obviously, the blind simulations provided rather good results for the elastic run and did not match experimental results as the nonlinearities increased. The blind hypotheses tend to overestimate the observed eigenfrequencies which means that the Young's modulus reduction needs to be higher than the one considered beforehand.

Run	f1 (Hz)	f2 (Hz)	f3 (Hz)
#7 (Num)	6.2	9.7	20.6
#7 (Exp)	6.1	7.8	16.5
#19 (Num)	5.1	8.1	17.2
#19 (Exp)	2.8	4.4	9

Table 7: comparison of eigenfrequencies between num vs. exp

3.6.2. Acceleration response spectra

The acceleration response spectra are compared between the numerical and experimental results in Figure 10 and Figure 11. The acceleration spectra are plotted at the control point D (top of the mock-up).

- for run#7, it is seen that the position of the peaks is rather well estimated (due to the good approximation of the main eigenfrequencies – the result is not that good for the third frequency). However, the amplitude of the peaks are overestimated in the numerical model meaning that the damping level needs to be increased in the model.
- for run #19, the same observations are made for the amplitudes of the peak values. In addition, we see that the model fails at reproducing the shift to the left due to the damage and the associated frequency drop.

However, the results of the simulation demonstrate the functionality of the numerical model. Indeed, the uncertainties of the input parameters and the boundary conditions are considered to have effects on the numerical results. For this reason, the uncertainty propagation is proposed, and the Bayesian updating approach is applied to update the uncertainties parameters based on the available measurements of the experiment.

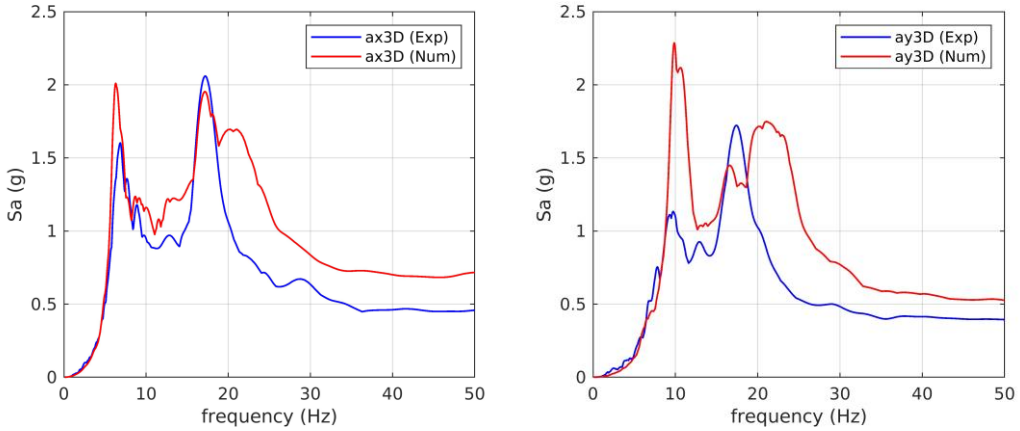

Figure 10: acceleration response spectra (run #7)

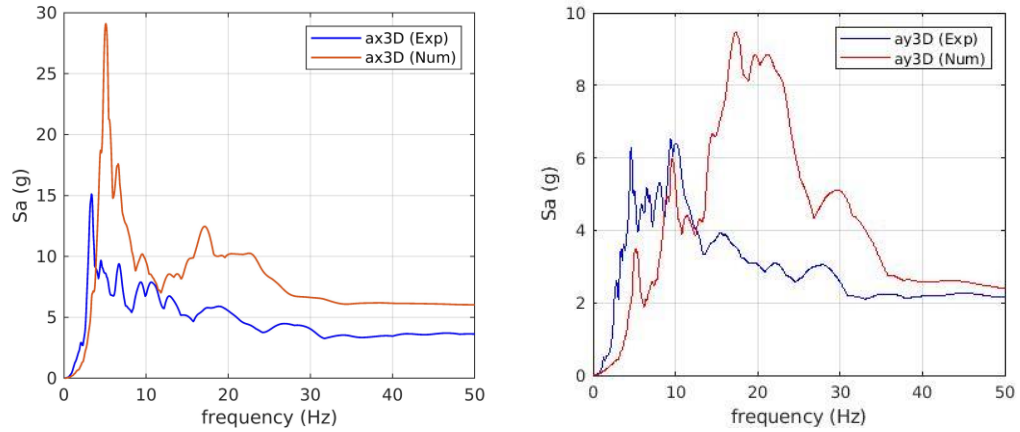

Figure 11: acceleration response spectra (run #19)

4. Theory of metamodeling and Bayesian updating

4.1. Polynomial Chaos Expansion

From a conceptual point of view, any continuous input–output map can be approximated by a Polynomial Chaos Expansions (PCE) surrogate model, which consists of a truncated series expansion formed by orthonormal polynomials (Ghanem, 1991):

$$Y(X) \approx \check{Y}(X) = \sum_{\alpha \epsilon A} a_\alpha \, \Psi_\alpha(X)$$

Where $A \subset N^d$ is a set of multi-indices, α the PCE coefficients and Ψ_α the associated tensorized polynomial term defined by: $\Psi_\alpha(X) = \prod_{i=1}^{d} \Psi_{\alpha_i}(X_i)$ with Ψ_{α_i} is the univariate polynomial of degree α_i.

In this work, the PCE coefficients are computed with the procedure based on the Least Angle Regression algorithm (LARS). The maximal polynomial order is set at 8. However, a lower order can be obtained if it is sufficient to get a good fit based on the so-called Leave One Out Cross validation error method. For the sake of illustration, a representative example of metamodels corresponding to run # 9 are provided in the appendix 11.1.

4.2. MCMC Bayesian updating

4.2.1. General framework of probabilistic models

Let be $(\Omega, \mathcal{F}, \mathbb{P})$ be a probability space. One considers a mathematical model $M\,(X,t)$ (analytical or numerical), representing the temporal evolution of a given system taking values in the space $\mathbb{R}^N$, and depending of m input parameters gathered in a random vector:

$$X : \Omega \longrightarrow D_X \subset \mathbb{R}^m$$

The uncertainties on input parameters are represented by a prior probability density function π_X.

Then, the model response Y is also a random vector:

$$Y(t) \; = \; M\,(X,t)$$

This setup defines a probabilistic model.

One considers a set of Nobs observations Y_{obs} = (y_1,…, y_{Nobs}) of the model response obtained at the corresponding instants (t_1,…, t_{Nobs}) . Then, model predictions M (X) differ from observations through a discrepancy ε_i:

$$y_i \; = \; M\,(X,t_i) \; + \; \varepsilon_i$$

This term ε_i comes not only from measurement error, but also from the model error since models are always simplified descriptions of real systems.

For the sake of simplicity, the model/measurement discrepancy is supposed to follow a zero mean Gaussian distribution $\mathcal{N}$ hereafter. That means that the conditional distribution of observations with respect to input parameters reads:

$$Y_i|X \; = \; x \; \sim \; \mathcal{N}\,(M\,(x,t_i), C)$$

with C the covariance matric of the model/measurement discrepancy.

This reformulates in terms of PDF as follows:

$$\pi_{Y_i|X}\,(\,y,x,t_i) \; = \; \varphi_C\big(y \; - \; M\,(x,t_i)\big)$$

with $\pi_{Y_i|X}$ is the conditional PDF of observations, and φ_C is the density of the distribution $\mathcal{N}(0,C)$.

4.2.2. Bayesian inverse problem and MCMC algorithms

Using Bayes' theorem, the posterior probability density function π_X^* of input parameters could be written as a function of the prior PDF (Berveiller et al., 2012; Tarantola, 1987):

$$\pi_X^*(x) = c\,\pi_X(x)\,\mathcal{L}(x;\,Y_{obs})$$

Where:

$$c = \frac{1}{\int_{D_X}\pi_X(x)\mathcal{L}(x;\,Y_{obs})dx}$$

is a normalization constant also known as Bayesian integral, and $\mathcal{L}(x, Y_{obs})$is the likelihood of the observations equal to:

$$\prod_{i=1}^{N_{obs}}\pi_{Y_i|X}(y, x, t_i)$$

In practice, there are several ways to calculate the posterior density of input parameters. Markov Chain Monte Carlo (MCMC) simulations are often used to determine this density (Tarantola, 1987). They consist of constructing a Markov Chain over the input parameters space, which behaves asymptotically as the posterior density of interest (Perrin, 2008). In this context, the Random Walk Metropolis–Hastings (RW-MH) algorithm (Hastings, 1970) constitutes the basis of MCMC algorithms. Given a Markov chain length NMCMC, this algorithm could be described as follows. First, an initial realisation x_0 of the input X is randomly chosen. At iteration k from a realisation x_k, a candidate point $\tilde{x}$ is drawn by making a translation from x_k with a zero-mean random vector, usually Gaussian or uniform. Then, the candidate is accepted with a probability equal to:

$$\alpha(\tilde{x}, x_k) = min(1, \frac{\mathcal{L}(\tilde{x};\,Y_{obs})}{\mathcal{L}(x_k;\,Y_{obs})})$$

The iterations are pursued until reaching the Markov chain length N_{MCMC}.

5. Global Bayesian updating strategy on SMART mock-up

In Figure 12 we show the global methodology of applying Bayesian updating to the SMART2013 mock-up's behaviour. Each calculation of eigenfrequencies requires about 2 minutes and each computation of the full transient elastic analysis requires about 6 minutes. Accordingly, the use of Markov Chain Monte Carlo (MCMC) during the Bayesian updating is expected to be a time-consuming process. To overcome this issue, the construction of Metamodels is proposed. Thus, the Metamodel is a mathematical function, and is constructed through the polynomial chaos expansion (PCE) equations (Berveiller M. L., 2012; Berveiller M. S., 2006; Blatman & Sudret, 2011; Blatman G. &., 2010). Afterward, the Bayesian approach calls directly to the Metamodel to update the uncertainties parameters with a comparable output to those obtained experimentally. In this work, we focus only on the updating of inputs' parameters based on measured eigne frequencies and the accelerations response spectra at the control point D (top of the structure). Also, to optimize the updating process further, the Bayesian updating is realized in two steps: first we update Young's modulus to get the right global eigenfrequency of the structure and then we update, after fixing the mean values of the Young's modulus, the damping ratios to get the peaks of acceleration response spectra at the main eigenfrequencies of the structure (Figure 13).

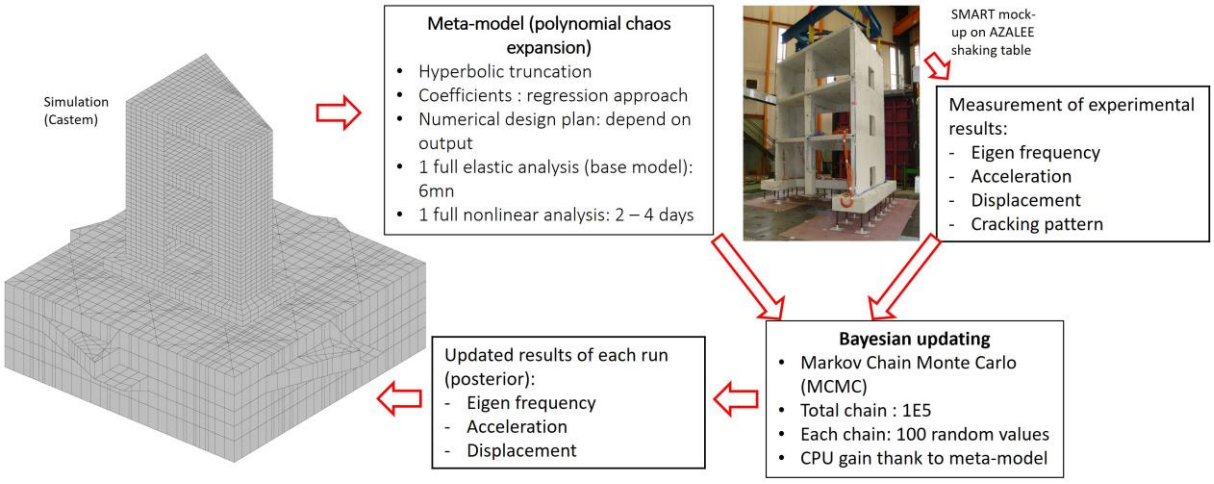

Figure 12: methodology of Bayesian on SMART mock-up

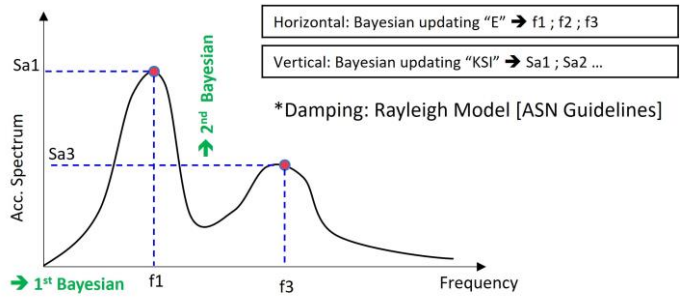

Figure 13: scope of Bayesian updating

In Figure 13, the 1st Bayesian updating aims at identifying the Young's modulus (E_c) of concrete to get a good estimation of eigenfrequencies (f_1; f_2; f_3), and to shift the curve horizontally. In Figure 14, we consider two configurations:

- Configuration 1 is to update only the Young's modulus of three elements of the foundation; this is limited to the linear elastic runs (#7; #9 and #11). The gaol is to better model the shaking table and the mock-up interactions.
- Configuration 2 concerns the nonlinear runs (#15; #17 and #19) where the cracks appear progressively in the structure. Therefore, the updating of Young's modulus in each run depends on the cracking state of the different structural elements.

It is worth mentioning that we use the same metamodel for both configurations as both are covered.

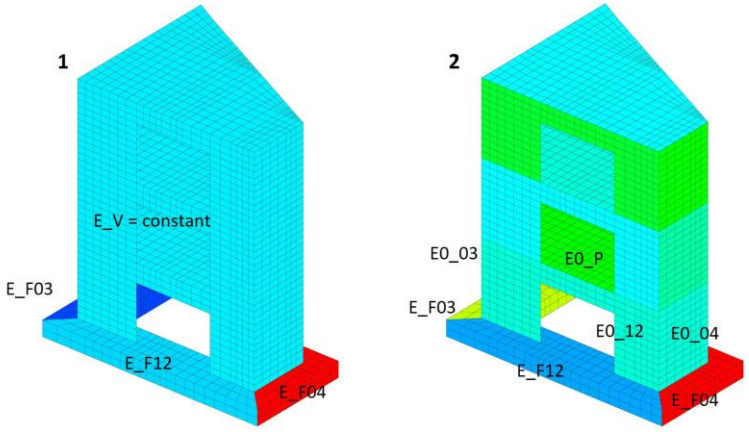

Figure 14: configuration of 1st Bayesian updating step

In Figure 13, the 2nd Bayesian updating aims at identifying the reduced damping ratios (ξ1; ξ2) for Rayleigh model depending on the observed cracking state. So, it is not possible to have one metamodel covering all runs. We need instead to develop a separate metamodel for each nonlinear run. Also, each meta model takes into account the updated values of the Young's modulus from the previous step.

6.Application to elastic and nonlinear cases

6.1. Elastic runs #7 #9 #11

6.1.1. Updating of eigenfrequencies

6.1.1.1. Global Meta model

A numerical design plan is proposed to cover all possibilities of most probable Young's modulus distributions (both for prior and posterior estimations). In Table 8, 12 parameters of Young's modulus for walls and slabs and 3 parameters of Young's modulus for the foundation are considered. The distribution of Young's modulus values E_0 at floor 0 is depicted in Figure 14. E_1 and E_2 refer to the groups of Young's moduli of floor 1 and 2. E_f refer to the Young's modulus of foundation elements. The numerical design plan is constructed using a range of values generated randomly (uniform distribution in Figure 15) between 0.2 GPa and 50GPa. It is worth mentioning that due to the large number of input parameters (15), the computation of PCE reaches about 20 000 terms of the polynomial function.

parameter	uniform	Remark
$E0_v$: $E0_{12}$; $E0_{03}$; $E0_{04}$; $E0_p$	2GPa – 50GPa	8000 set of random values for 15 structural elements
$E1_v$: $E1_{12}$; $E1_{03}$; $E1_{04}$; $E1_p$		
$E2_v$: $E2_{12}$; $E2_{03}$; $E2_{04}$; $E2_p$		
E_{F12}: E_{F03}; E_{F04}	0.2GPa – 50GPa	

Table 8: Young's modulus proposed in numerical design plan

Each random set of Young's modulus values provides us with a set of three main eigenfrequencies. Then, a metamodel is constructed relating those eigenfrequencies with the Young's modulus values. In

Figure 17, Y(PCE) represent the results computed from the fitted metamodel whereas Y(true) are obtained directly by means of numerical simulations. It is observed that metamodel reproduces well the estimated eigenfrequencies (MSE=$\frac{1}{n}\sum_{i=1}^{n}\left(y_{pce,i}-y_{true,i}\right)^2$). With this metamodel, the use of MCMC during updating becomes accessible with a reasonable computational time.

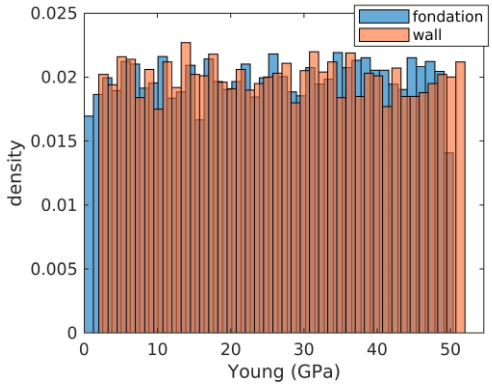

Figure 15: uniform distribution

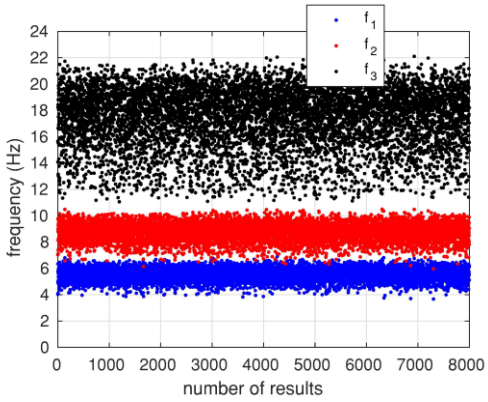

Figure 16: three modes of eigenfrequencies

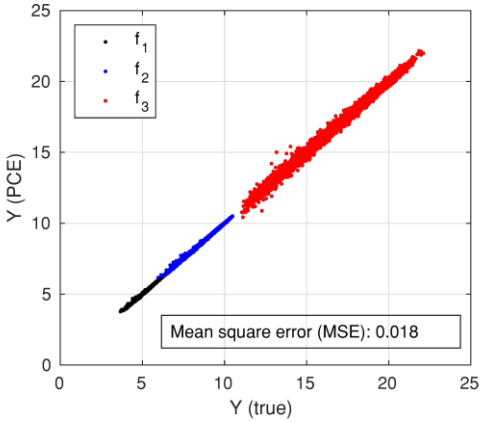

Figure 17: comparison of metamodel with numerical simulation results

6.1.1.2. Updated Young's modulus distributions

For the elastic runs (#7; #9; #11), no cracks are observed from an experimental point of view and the measured eigenfrequencies remain constant in those runs. Accordingly, we limit the Bayesian updating of Young's modulus to the three volumes of the foundation only (Figure 18).

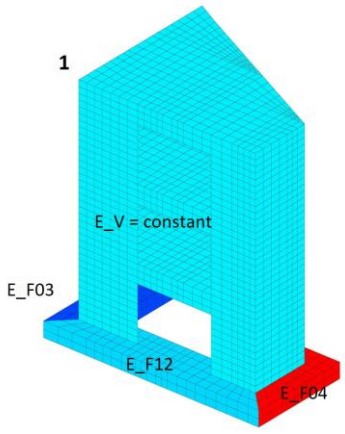

Figure 18: configuration of elastic runs

In Figure 19, the updated Young's modulus values, which is known as posterior distribution is illustrated along with the prior distribution. The prior distribution is supposed log-normal based on the measured results on the sample scale. After doing the Bayesian updating, it is observed that the posterior distribution shifts to the left, especially for E_{F12} and E_{F03}. The mean values and coefficients of variation of the prior and posterior are presented in Table 9. The posterior value of E_{F03} is reduced by about 42 times compared to the prior. This reduction is not due to the cracking (as we are within elastic behavior) but to the simplified way our modelling accounts for the interface between the mock-up and the foundation. In Figure 19, the comparison of eigenfrequencies estimated by prior and posterior is provided. We clearly notice the improvement of our estimations based on the updated Young's modulus in the foundation.

Prior/posterior: (MCMC=1e5 chains; 100 values/chain
E_V = 25700 MPa (constant)
E_{F12}: (μ = 25700 MPa / 4000 MPa ; Cov = 80%/83%)
E_{F03}: (μ = 25700 MPa / 600 MPa ; Cov = 80%/40%)
E_{F04}: (μ = 25700 MPa / 20000 MPa ; Cov = 80%/62%)

Table 9: prior and posterior properties of Young's modulus

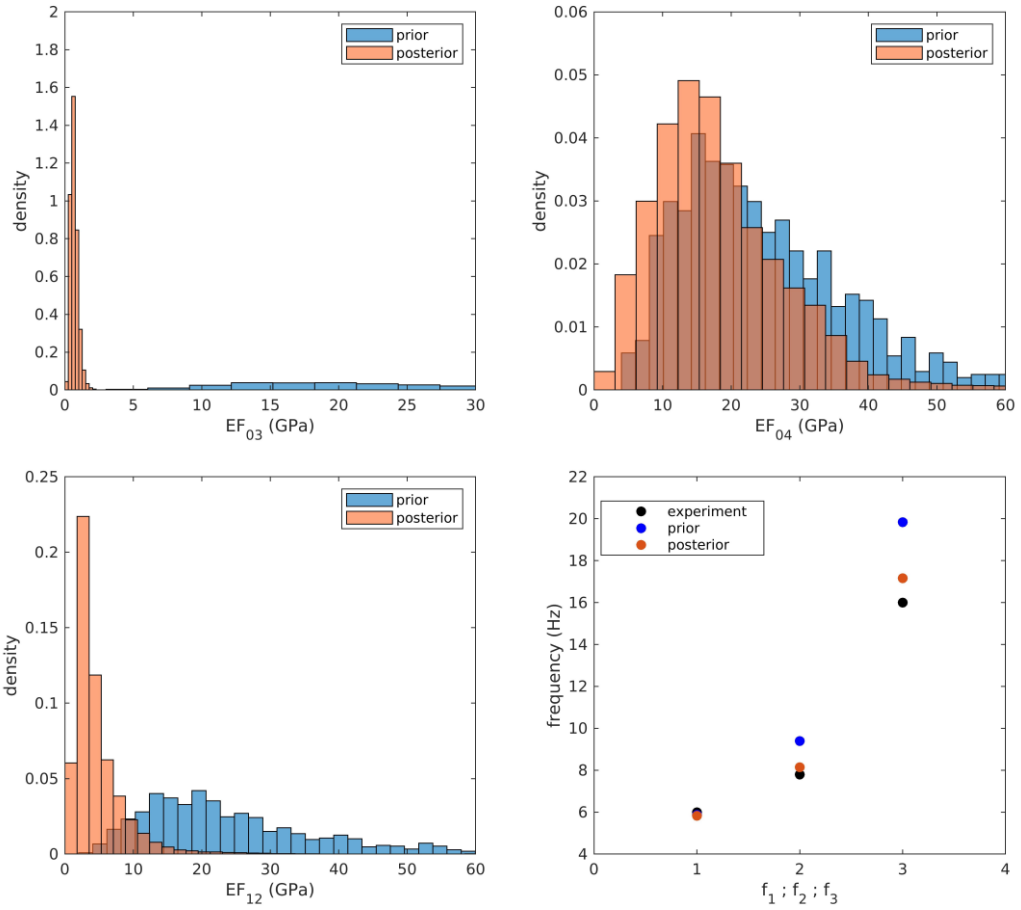

Figure 19: prior/posterior of Young's modulus and estimation of eigenfrequencies

6.1.2. Updating of acceleration spectra

6.1.2.1. Metamodel

In this 2nd Bayesian updating step, metamodels are constructed for each run. The proposed numerical design plan is provided in Table 10. The damping ratios, ξ_1 and ξ_2, are generated according to a uniform

distribution with boundaries between 1% to 30%. Each metamodel is based on 100 simulations. The outputs of interest are the spectral accelerations at the control point D. In Figure 20, we see that the estimations from the metamodel provides good agreement with those of the exact numerical simulation. It is seen that the mean square error is relatively small, and all the dot points are slightly scattered along the diagonal.

parameter	uniform	Remark
ξ_1	1% – 30%	100 random values for each run
ξ_2		

Table 10: damping ratio proposed in numerical design plan

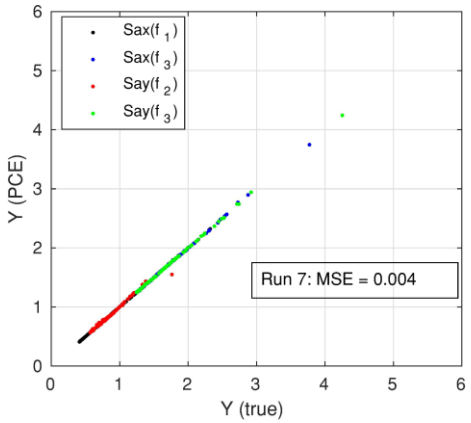

Figure 20: comparison of metamodel vs. numerical simulation results (for run #7)

6.1.2.2. Updated damping ratios distributions

In Table 11, the prior and posterior values of damping ratios are presented. Due to the limited knowledge of the prior distribution for the damping ratios, we consider here a uniform distribution varied between 1% to 3% is selected. This corresponds to a mean damping of 2% and a coefficient of variation of 50%. As a reminder, ξ_1 and ξ_2 correspond to damping ratios at f_1 and f_3 frequencies respectively. The posterior properties show that ξ_1 varies between 1.4% to 3.8% and ξ_2 varies from 12% to 18% for all the elastic runs #7; #9 and #11. One should note that, to ensure an update of the domains boundaries when necessary, the initial domain of interest where we try to identify our candidate x_k was extended to [1%-30%].

prior	Posterior
Run #7: U(1% - 3%)	ξ_1 : (μ=3.8%; cov=13%)
	ξ_2 : (μ=12%; cov=9%)
Run #9: U(1% - 3%)	ξ_1 : (μ=1.4%; cov=16%)
	ξ_2 : (μ=18%; cov=6%)
Run #11: U(1% - 3%)	ξ_1 : (μ=2.8%; cov=11%)
	ξ_2 : (μ=14.5%; cov=5%)

Table 11: prior and posterior properties of damping ratios

In Figure 21, the distributions of prior and posterior of the damping ratios are illustrated. One can notice the reduction of uncertainties for the posterior estimations based on the knowledge we have from in situ measurements.

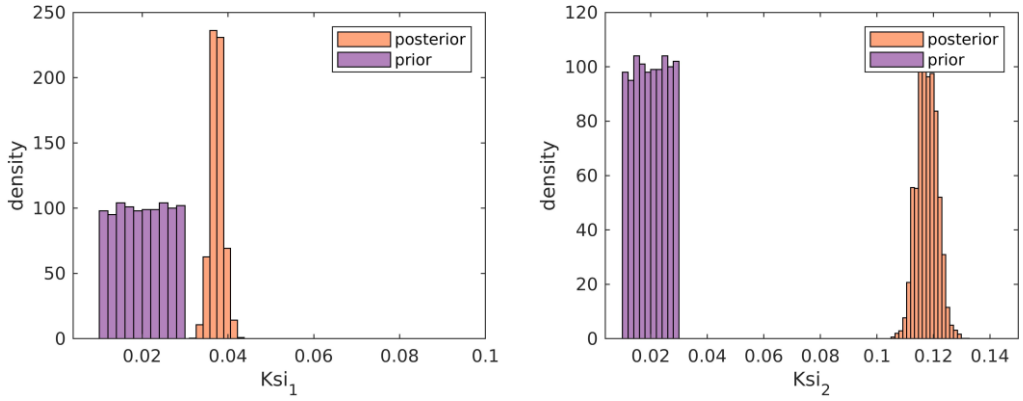

Figure 21: prior and posterior distribution of damping ratios, ξ_1 ; ξ_2 (run #7)

6.1.2.3. Verification of the results at another control point B

So far, the updated parameters are obtained based on measurements at the control point D only in addition to the eigenfrequencies. To verify the accuracy of the updating in other positions of the model, we select the point B (illustrated in Figure 22) to check the reduction of gaps at this point as well. It is seen that the black curves (after the 1st step of updating) provides peaks at accurate frequencies and that the red curves (after 1st and 2nd updating steps) represented for the simulation with all the updated parameters have a good agreement with those of the blue curves from the experiment. Besides, one can see the reduction of uncertainties (grey to green areas) as the updating is applied. In addition, even though the Bayesian updating is only applied based on the results in point D, the comparison of results at point B in Figure 23 proves that the improvement is rather verified for other points as well (even though they were not considered during the updating phase). Results are shown here for run #7 whilst the rest of results is illustrated in the appendix.

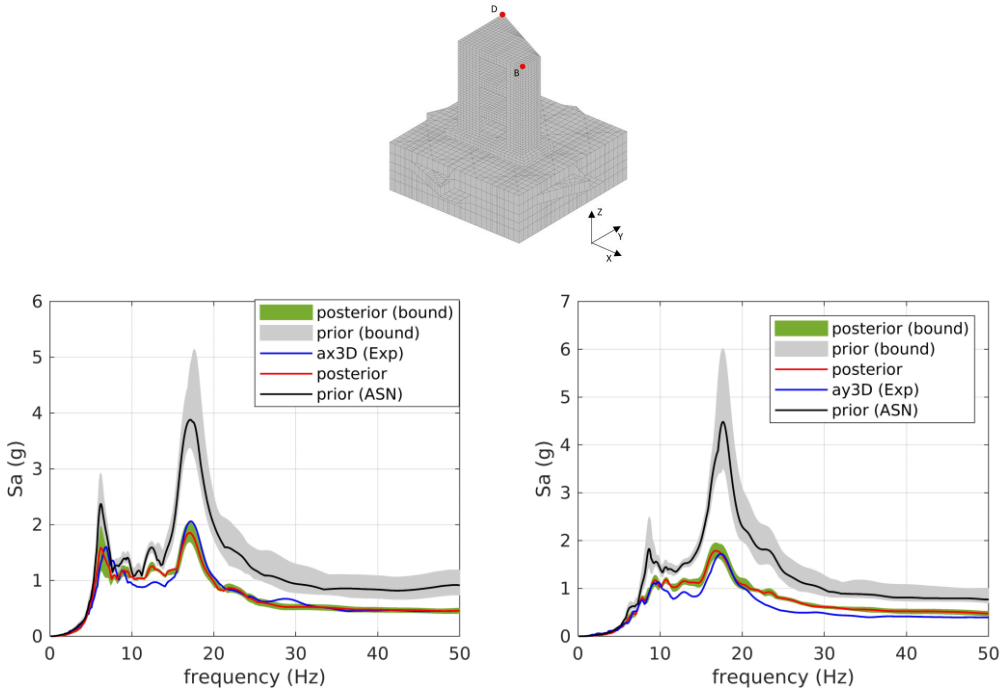

Figure 22: acceleration response spectra at control point D (run #7)

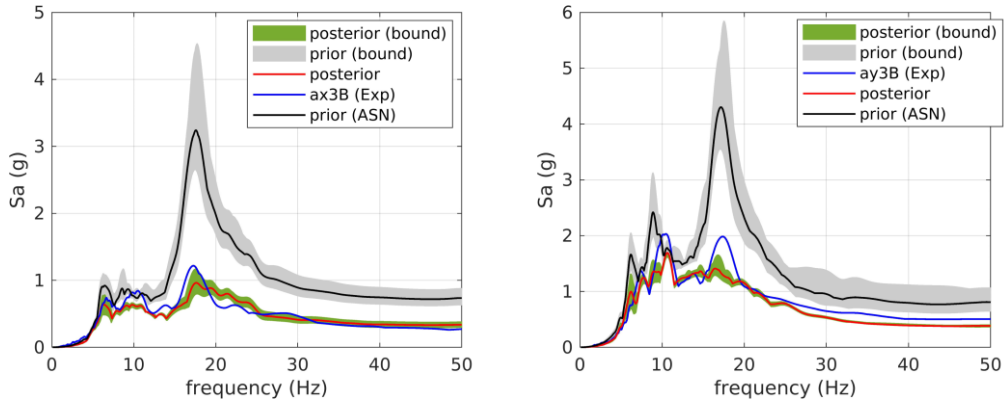

Figure 23: acceleration response spectra at point B (run #7)

6.2. Nonlinear run #19

6.2.1. Updating Eigenfrequencies

The 1st Bayesian updating in nonlinear runs (#15; #17; #19) is performed successively after the elastic runs. For example, the posterior Young's modulus of run #11 is used as the prior properties for the 1st Bayesian updating of run #15, the posterior of run #15 is used as a prior of run #17 and the posterior of run #17 is used as the prior of run #19. In this section, only the run #19 is presented and the rests (#15 and #17) are detailed in the appendix.

In Figure 24, Figure 25 and Figure 26, the prior and posterior distribution of Young's modulus are illustrated for each structural element. Only the structural elements that are cracked (experimental observations) are activated in the Bayesian updating process. Obviously, the posterior Young's modulus shift to the left, which means that the updated Young's modulus is reduced compared to the prior for the cracked elements. In Figure 26, a comparison of prior vs. posterior eigenfrequencies is provided. The improvement is clear for posterior results. In Table 12 and Table 10, the parameters of prior and posterior distribution are presented. The Young's modulus of the walls, V_03 and V_04 on the second and third floor are considered as constant because there are no cracks observed experimentally.

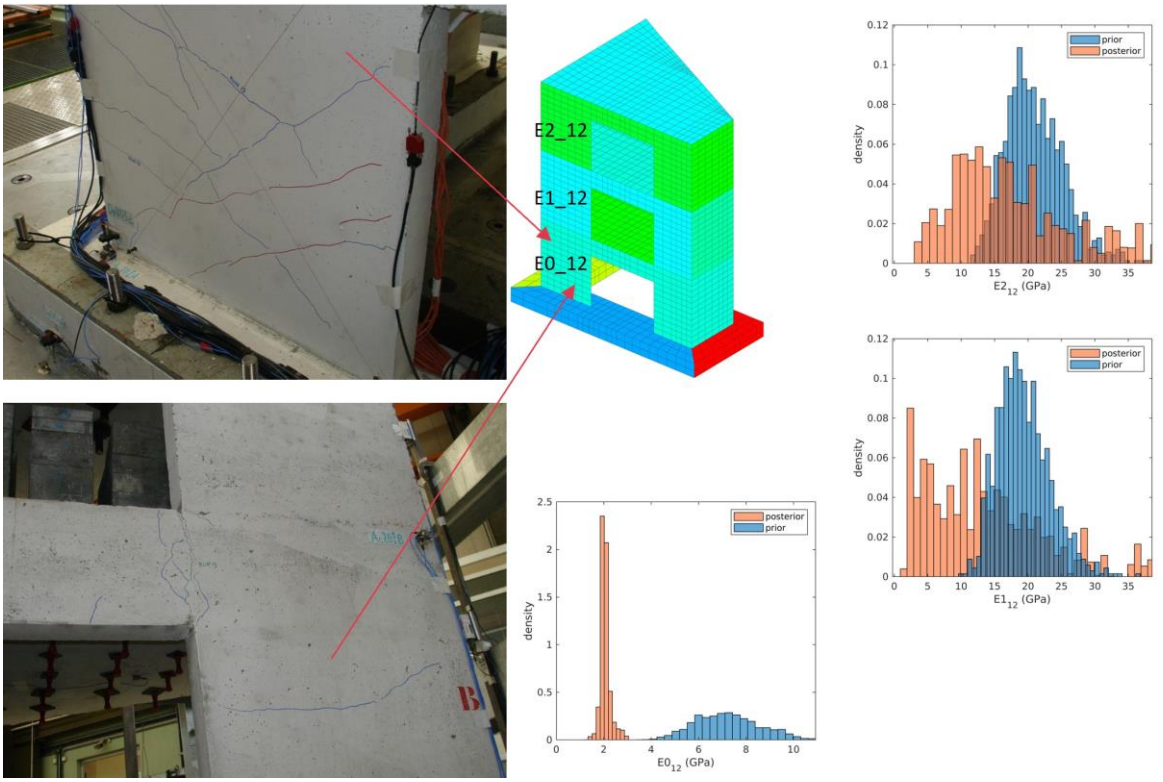

Figure 24: prior/posterior of Young's modulus distribution on wall (V_12)

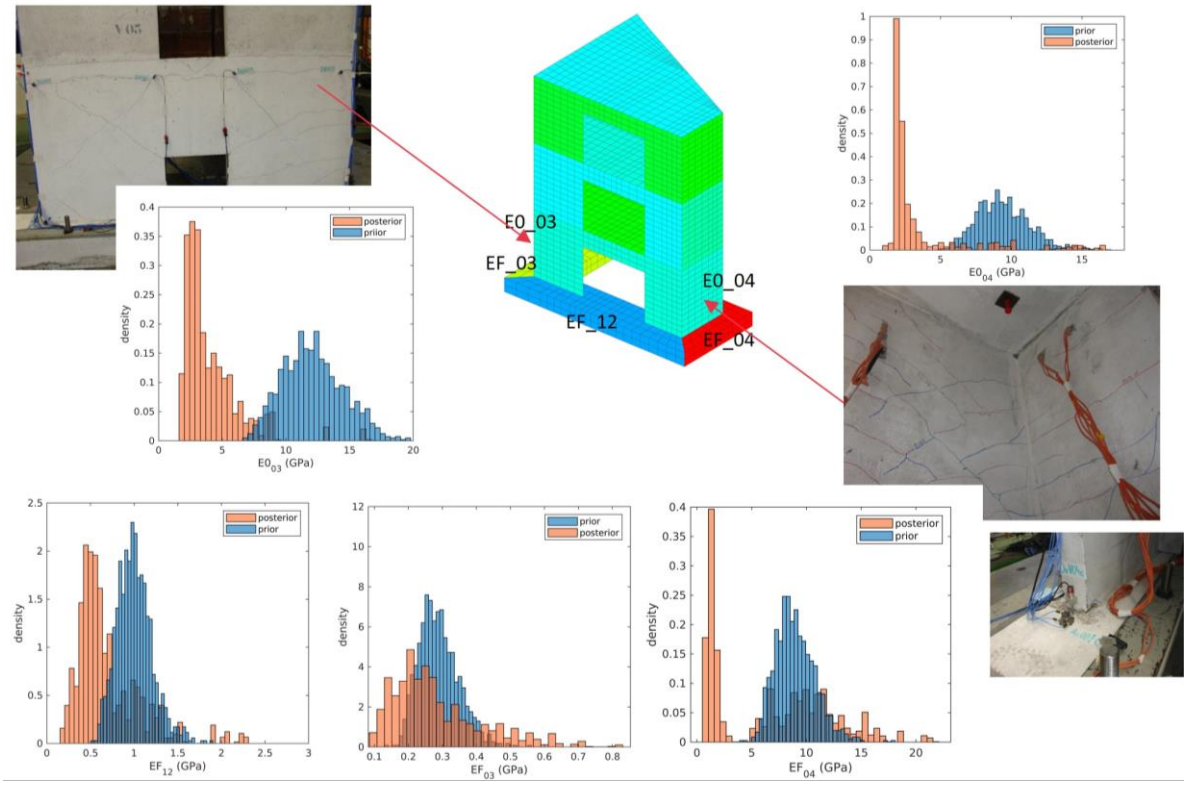

Figure 25: prior/posterior of Young's modulus distribution on walls and foundation

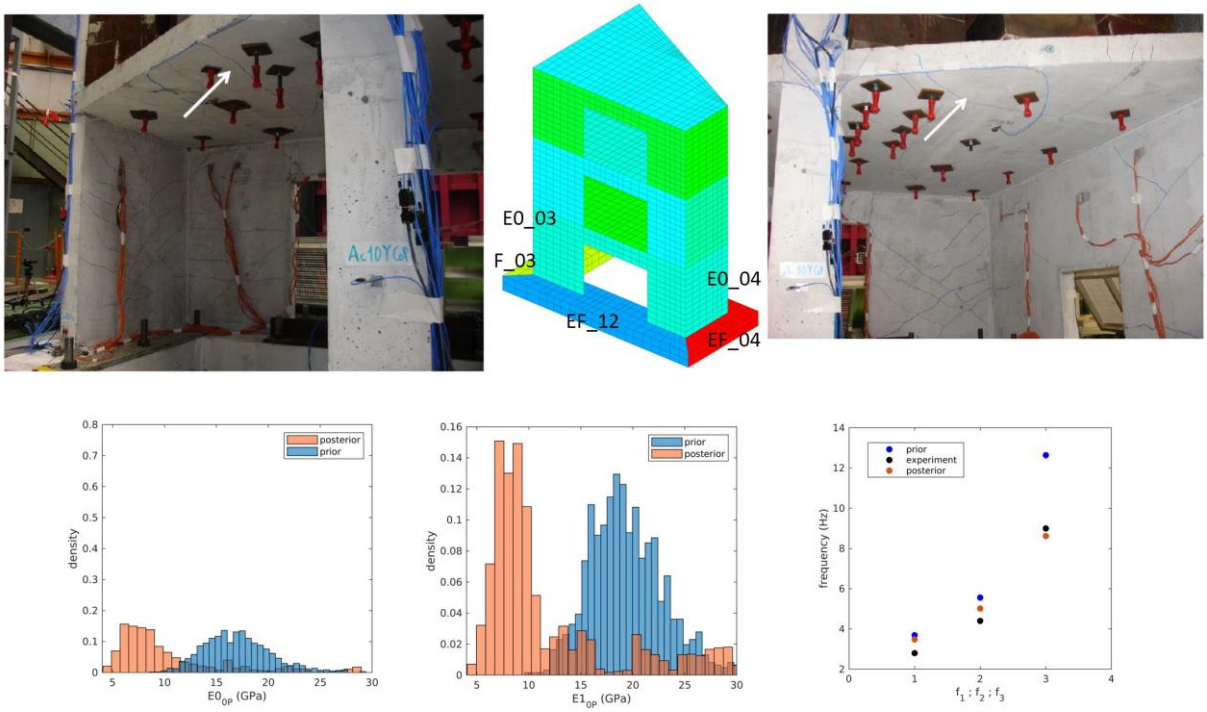

Figure 26: prior/posterior of Young's modulus distribution on the slabs

Prior/posterior: (MCMC=1e5 chains; 100 values/chain)	Remarks
$E0_{12}$: (μ = 7200 MPa / 2200 MPa ; Cov = 20%/43%)	-
$E0_{03}$: (μ = 12000 MPa / 4100 MPa ; Cov = 20%/56%)	-
$E0_{04}$: (μ = 9400 MPa / 3800 MPa ; Cov = 20%/96%)	-
$E0_{P}$: (μ = 17000 MPa / 10500 MPa ; Cov = 20%/56%)	-
$E1_{12}$: (μ = 19400 MPa / 13500 MPa ; Cov = 20%/65%)	-
$E1_{03}$: 25700 MPa (constant)	No crack
$E1_{04}$: 25700 MPa (constant)	No crack
$E1_{P}$: (μ = 19600 MPa / 14000 MPa ; Cov = 10%/69%)	-
$E2_{12}$: (μ = 21000 MPa / 18700 MPa ; Cov = 10%/56%)	-
$E2_{03}$: 25700 MPa (constant)	No crack
$E2_{04}$: 25700 MPa (constant)	No crack
$E2_{P}$: 25700 MPa (constant)	No crack
E_{F12} : (μ = 1000 MPa / 700 MPa ; Cov = 10%/54%)	-
E_{F03} : (μ = 288 MPa / 285 MPa ; Cov = 20%/56%)	-
E_{F04} : (μ = 9000 MPa / 6700 MPa ; Cov = 20%/77%)	-

Table 12: prior and posterior of Young's modulus

6.2.2. Updating acceleration spectra

6.2.2.1. Metamodel

After the 1st Bayesian updating step, the metamodel for the 2nd Bayesian updating step is constructed following the same strategy as in the elastic runs or cases. Only the damping ratios are randomly generated from Table 10 (we use the Young's modulus values resulting from the previous updating step). In Figure 27, the comparison of the peaks of acceleration spectra at point D estimated using the metamodel and the exact numerical simulation is given. The scattering of results along the diagonal is very limited.

6.2.2.2. Updated damping ratios distribution

The 2nd Bayesian updating step is performed to identify the damping ratios based on the measured acceleration response spectra. In Table 13, the prior and posterior properties of damping ratios are provided. On the nonlinear runs (#15; #17; #19), the updated damping ratios are varied between 1% - 12% for ξ_1 and 16% - 28% for ξ_2. These results differ from the 7% to 10% damping ratios one can find in some regulatory codes. However, it is worth mentioning that these regulatory codes remain conservative, and they are more suited for design analysis and not best estimate calculations. In Figure 28, the distributions of prior and posterior are illustrated as well. The posterior distributions of ξ_1 and ξ_2 tend to a log-normal distribution while the initial prior distribution is supposed as a uniform distribution.

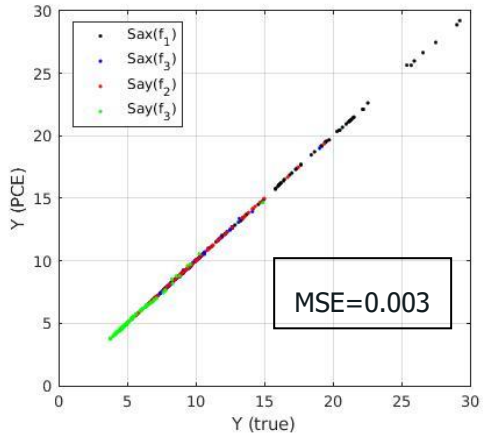

Figure 27: comparison of Metamodel with numerical simulation run #19

prior	Posterior
Run #15: U(3.5% - 10.5%)	ξ_1 : (μ=1%; cov=1.3%)
	ξ_2 : (μ=16%; cov=65%)
Run #17: U(3.5% - 10.5%)	ξ_1 : (μ=6%; cov=12%)
	ξ_2 : (μ=20%; cov=24%)
Run #19: U(3.5% - 10.5%)	ξ_1 : (μ=12%; cov=1.4%)
	ξ_2 : (μ=28%; cov=1.1%)

Table 13: prior and posterior of damping ratios (runs #15; #17; #19)

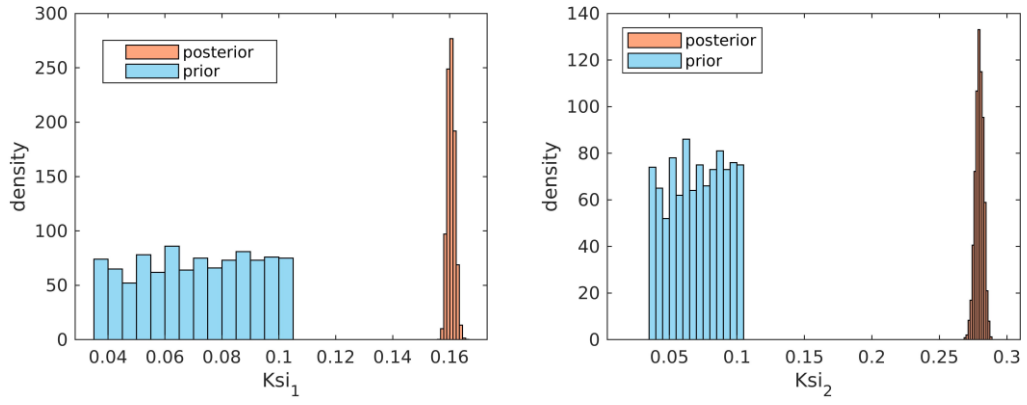

Figure 28: prior and posterior distribution of damping ratios, ξ_1 ; ξ_2 (run #19)

6.2.2.3. Verification of the results

As in the previous elastic case, the comparison of acceleration response spectra at points D and B are illustrated in Figure 29 and Figure 30. The improvement of acceleration response spectra is observed.

The updated damping ratios have significantly modified and adjusted the peak of acceleration response spectra at the corresponding eigenfrequencies.

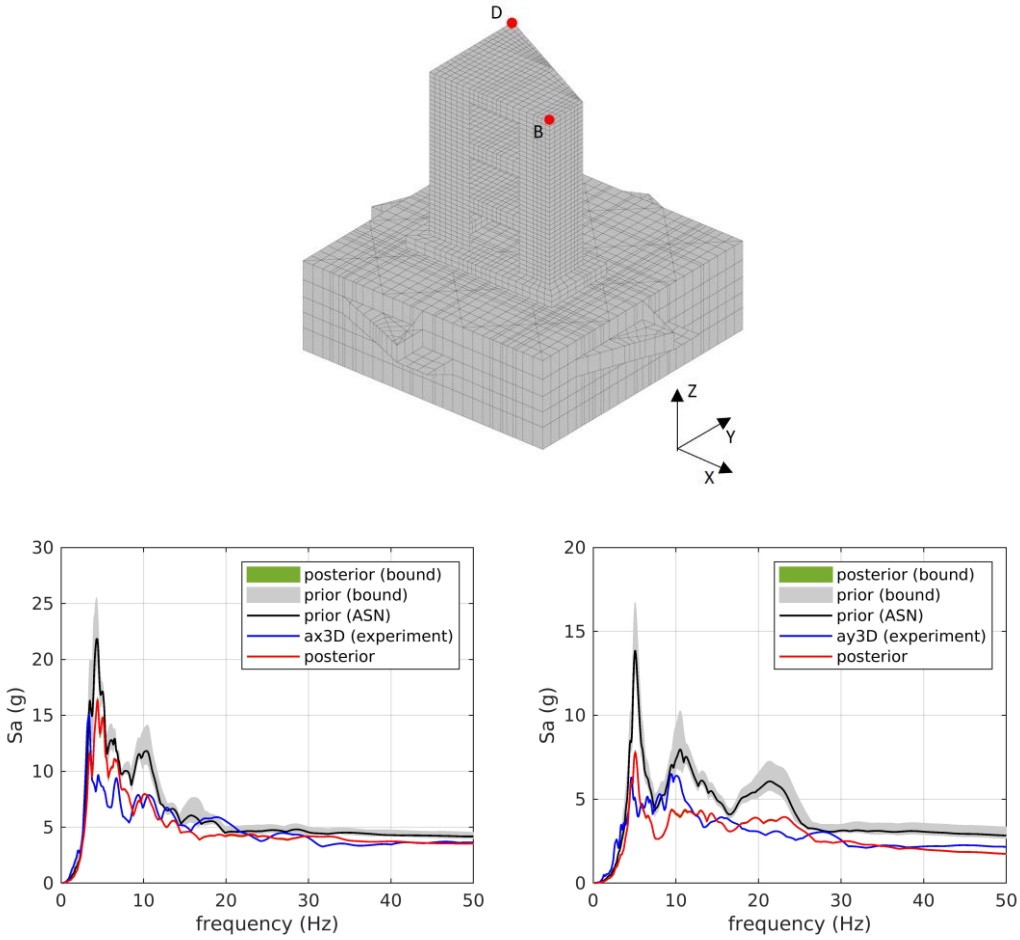

Figure 29: acceleration response spectra at control point D (run #19)

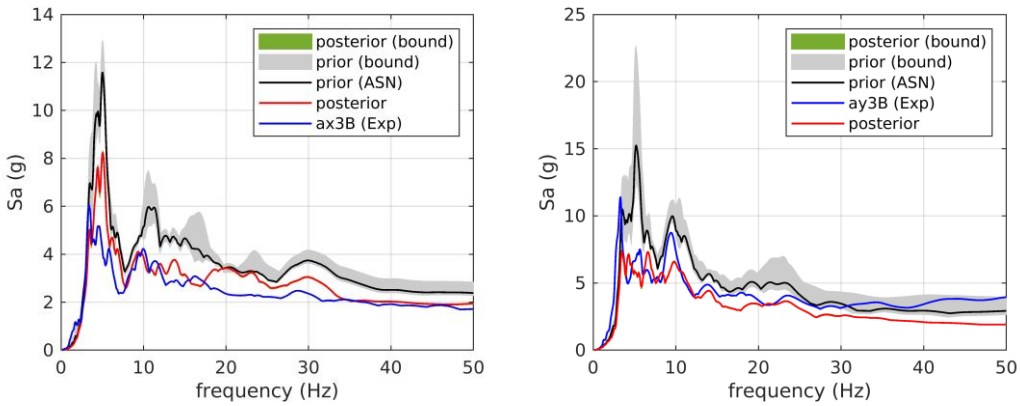

Figure 30: acceleration response spectra at point B (run #19)

6.3. Overview of all results

The overall results of the updated parameters are presented in Figure 31 and Figure 32. For the sake of comparative analysis, the common design regulatory (ASN, 2006) guidelines proposed for elastic equivalent simulation are plotted as well. The ratios of effective Young's modulus are illustrated for different runs. It is observed that from nonlinear runs (#15; #17; #19), the ratios of effective Young's modulus for cracked elements can be way larger than 2 depending on the PGA level (Figure 31). As

observed from the SMART2013 mock-up, most of the cracks are concentrated on the walls of the 1st floor ($E0_{12}$; $E0_{03}$; $E0_{04}$), and those posterior reduction factors of Young's modulus vary between 6 to 12.

The evolution of the damping ratios at different runs are described in Figure 32. From run #7 to run #17, ξ_1 remains under the value proposed by regulatory guidelines (7%) for the elastic equivalent simulation. However, at run #19 (PGA=1.1 g), the updated damping ratio goes above the value of regulatory guideline. These results underlines the necessity of having coherent damping ratios with the expected damage state and also the difficulty of estimating blindly such expected damage state.

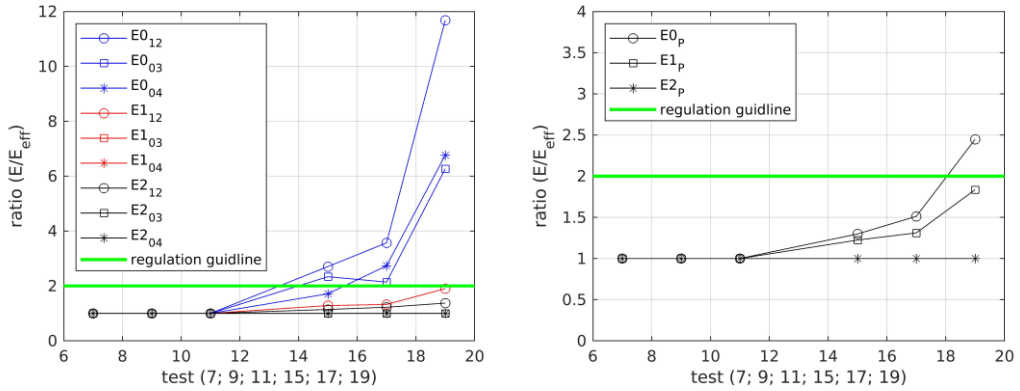

Figure 31: Effective Young's modulus reduction factor (left: wall; right: slab)

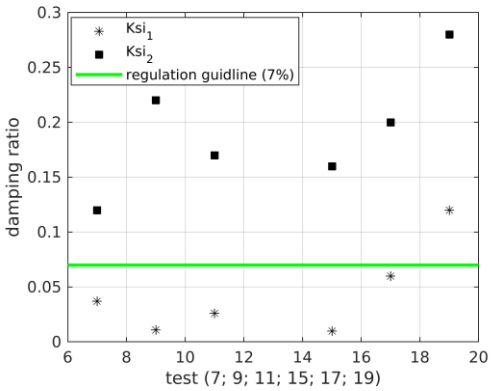

Figure 32: updated damping ratios for different runs

7. Updating of fragility curves

7.1. Principle of fragility computation

The fragility curve is computed based on the statistical regression approach relating the drift or the spectral acceleration (EDPs of interest) and the PGA (the considered IM) to which an error function is added to account for the scattering of true values around the fitted regression model. Such function is supposed to follow a centred normal distribution with a standard deviation σ_ε:

$$EDP = f_{regression}(PGA) + f_{err}(0, \quad \sigma_\varepsilon)$$

So, the fragility curve writes for each given PGA:

$$P(EDP \geq EDP_{lim}|PGA) = P\left(f_{err}(0, \quad \sigma_\varepsilon) \geq \left(EDP_{lim} - f_{regression}(PGA)\right) |PGA\right)$$

This method allows up to make interpolations and extrapolations for PGAs which have not been tested experimentally.

The first engineering demand parameter (EDP) to be considered is the spectral acceleration amplitude ($S_{a,N}$) at point D corresponding to the first peak at the 1st eigen frequency. The second EDP is the maximal nominal inter-storey drift (δ_n) at point D.

$$S_{a,N} = \sqrt{S_{a,X}^2 + S_{a,Y}^2} \qquad \delta_n = \sqrt{\delta_{X,max}^2 + \delta_{Y,max}^2}$$

In Figure 33, the post processing methodology of fragility curves is illustrated. Eventually, the updating of the fragility curves consists of considering prior and posterior regressions using prior and posterior EDPs vs. PGAs. For each regression, one gets a different value for the standard deviation σ_ε; then different probabilities of exceedance. Three confidence levels 5%, 50% and 95% are considered for each EDP vs. PGA regression function. By the use crude Monte Carlo method, using about 10^6 random realizations of the error function.

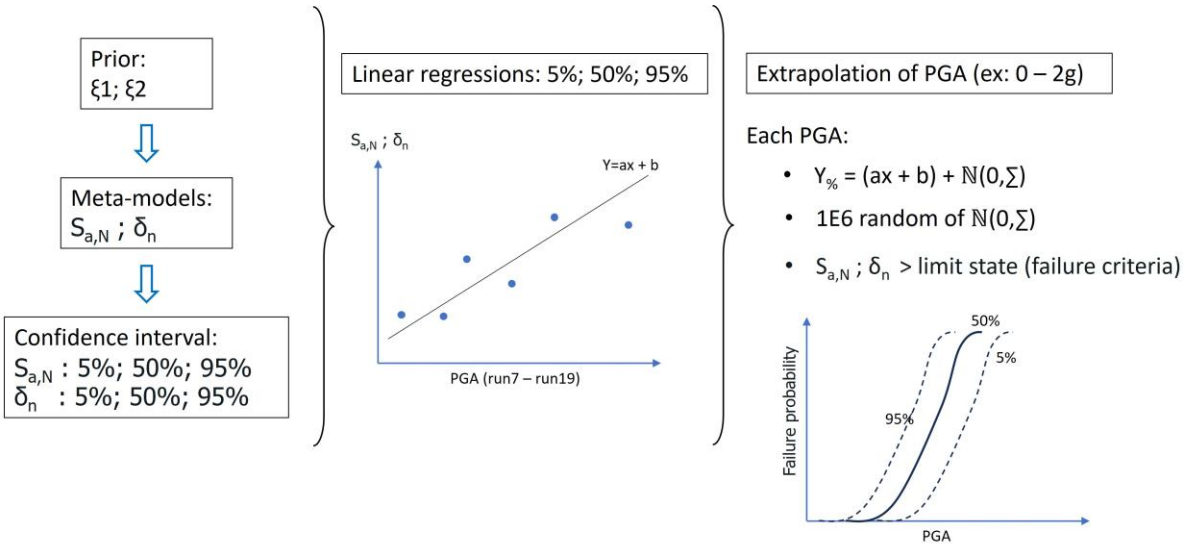

Figure 33 : computation of fragility curve method

7.2. Fragility curve based on spectral accelerations

To compute the fragility curve based on the acceleration response spectra, the threshold ($S_{a,lim}$) is set arbitrarily at 15g for the sake of illustration. The fitted linear models of prior and posterior are illustrated in Figure 34 for different fractiles. For each, the correlation coefficients of the fitted curve is above 98%.

As discussed, the uncertainty error of the fitted linear model is supposed to follow a normal distribution. The parameters of the normal distribution correspond to different cases of confidence levels are provided in Table 14, and those parameters are derived from the fitted linear model.

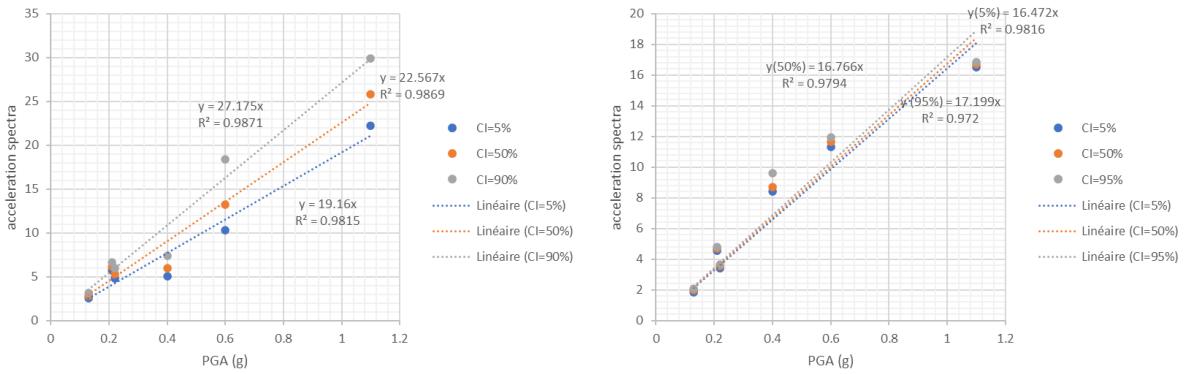

Figure 34: fitted linear model: spectral acceleration vs. PGA (left) prior (right) posterior

	prior	Posterior
5%	$\mathbb{N}(0, 1.6)$	$\mathbb{N}(0, 1.3)$
50%	$\mathbb{N}(0, 1.57)$	$\mathbb{N}(0, 1.4)$
95%	$\mathbb{N}(0, 1.87)$	$\mathbb{N}(0, 1.67)$

Table 14: prior and posterior error functions: spectral acceleration vs. PGA

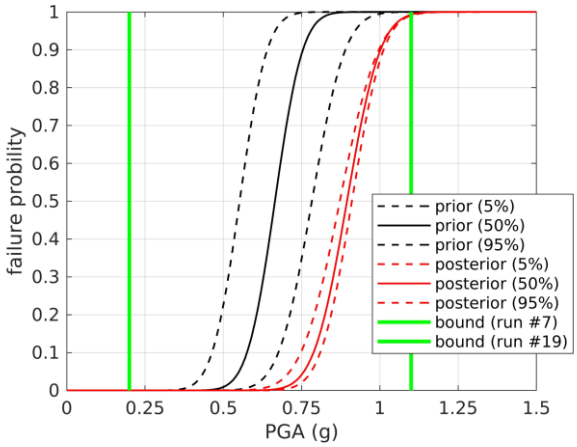

Figure 35: fragility curve for spectral accelerations

In Figure 35, the fragility curves of prior and posterior spectral accelerations are computed. The bandwidth between 5% to 95% is obviously reduced for the posterior obtained after Bayesian updating. The shift to the right is explained by the increase of our damping ratios for posterior calculations leading to lower spectral accelerations and hence less probabilities of failure.

7.3. Fragility curve based on inter-story drift

The fragility curves are constructed for two threshold values set at 4‰ and 6‰ for the sake of illustration. Similarly, to those presented in section 6.2, the fitted linear models are constructed for three confidence levels: 5%; 50% and 90%. In Figure 36, the example of a fitted linear model is illustrated. The uncertainty error of the fitted linear model is provided in Table 15.

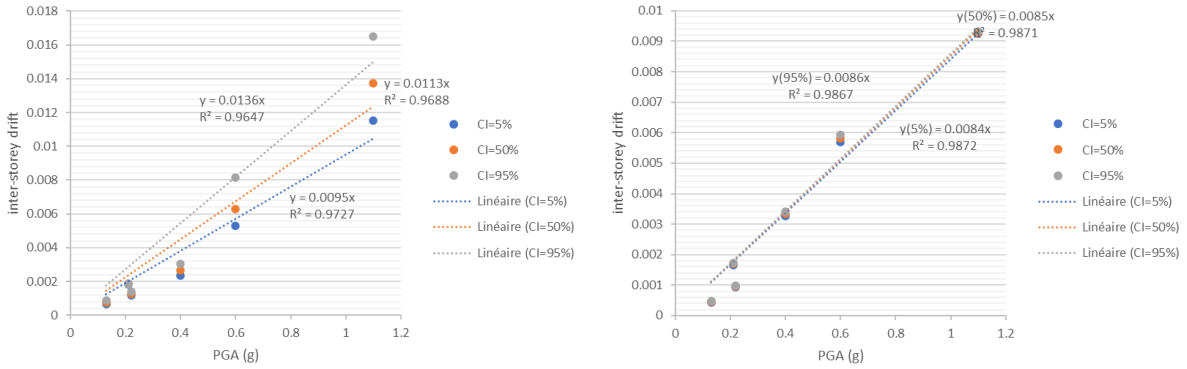

Figure 36: fitted linear model : drift vs. PGA (left) prior (right) posterior

	prior	Posterior
5%	$\mathbb{N}(0, 0.008)$	$\mathbb{N}(0, 0.00054)$
50%	$\mathbb{N}(0, 0.001)$	$\mathbb{N}(0, 0.00056)$
95%	$\mathbb{N}(0, 0.0013)$	$\mathbb{N}(0, 0.00058)$

Table 15: prior and posterior error functions: drift vs. PGA

In Figure 37, the fragility curves are computed for the two criteria. The bandwidth of the posterior fragility curve between 5%-95% is relatively small compared to the one obtained as a prior. Furthermore, the posterior fragility curves are shifted to the right for the same reason as in the case of spectral accelerations (related to damping hypothesis).

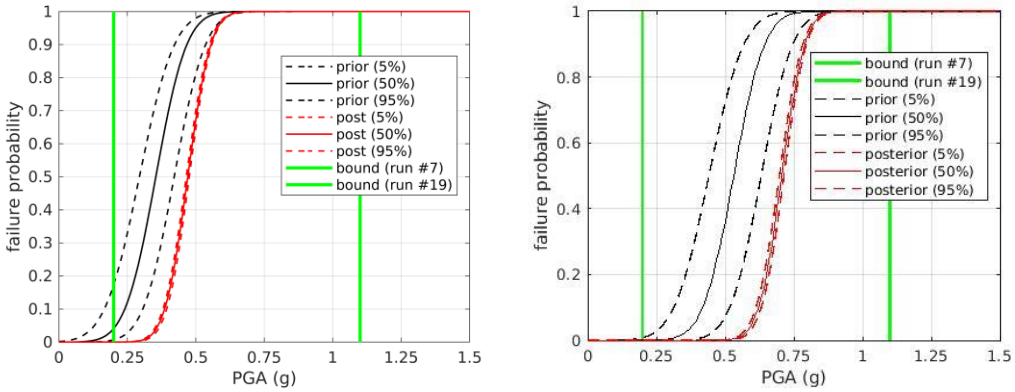

Figure 37: fragility curves for inter-story drift with a threshold at (left:4‰ ; right:6‰)

8. Conclusion

In this report, the methodology of Bayesian updating is developed and applied to the seismic behaviour of reinforced concrete structures through the case of SMART2013 mock-up. Even with the use of linear or linear equivalent constitutive models, it is shown that the coupling of metamodeling and Bayesian updating methods allows for a considerable computational time reduction. In this work, updating was geared towards the Young's modulus and damping ratio. However, one should understand that this can be applied to other inputs as well. Also, in this work, as we directly updated the inputs of our model, all EDPs of interest were calculated using standard uncertainty propagation methods such as basic (with no optimization) Monte Carlo method or Markov Chain Monte Carlo approaches. Eventually, the fragility curves were post processed in a straightforward way based on the application of stochastic metamodeling to link the EDPs of interest to the PGAs.

In the obtained results, the improvement of the estimations of eigenfrequencies and spectral accelerations was obvious coping with the difficulty of knowing blindly what values should be considered for each input. The physical trends were also met during the process such as the Young's modulus reduction and damping ratio increase with the resulting damage due to the seismic loads. The updating was also of interest to grasp a good modelling of the boundary conditions between the shaking table and the mock-up in an equivalent but satisfactory way. As far as fragility curves are concerned, and in addition to the improvement of results, the application of Bayesian updating clearly reduced the epistemic uncertainties for all studied cases (drifts and spectral accelerations).

Finally, one should note that the current updating methodology was applied within an equivalent linear framework. Future work would be geared towards the use of direct nonlinear models. The main challenge is, as often, related to the limitation of the computational cost considering adapted numerical design plan. Another possible improvement would be the application of the updating process to the fragility curves directly without going through the updating of the model's inputs. These points will be considered for future developments.

9. Applicability of the approach at an industrial scale

For any application of the Bayesian techniques, especially at the full structural scale, the availability of in situ data and measurements is a key element in the process. With limited data, the efficiency of the updating techniques as the Bayesian approaches becomes very limited. To cope with such constraint at the industrial scale, and as experimental data are scarce, the Bayesian updating techniques can be applied within different scopes. For instance, to illustrate the possible practical and operational applications, we can evoke three main and promising possibilities:

- the use of Non-Destructive Techniques (NDT) to quantify more objectively the properties of reinforced concrete at the structural scale and then propagate those uncertainties using an adapted model ;
- the updating of prior results (frequencies, spectral accelerations, drifts, etc.) that are based on linear equivalent analysis using data that are provided by calculations based on advanced nonlinear analysis. In this situation, nonlinear results play the role of reference results that the model should be updated according to (they replace the experimental measurements). Of course, to do so, one should have sufficient trust in the model's validity and reliability ;
- the updating of prior fragility curves (estimated using the strategy developed in this report or based on usual industrial methods such as the EPRI 3002012994 guidelines on this matter) based on post seismic feedback database such as the SQUG databases amongst others.

These topics remain of interest and shall be explored within a near future within on going and future R&D projects following METIS framework.

10. Bibliography

ASN (2016). Guide 2/01. Accounting for the seismic risk during the design of civil engeneering works of basic nucealr installations except those for the long-term storage of nuclear waste.

EPRI 3002012994. EPRI 3002012994 on the seismic Fragility and Seismic Margin Guidance for Seismic Probabilistic Risk Assessments.

B. Belletti, A. Stocchi, M. Scolari, F. Vecchi (2017). Validation of the parc-cl 2.0 crack model for the assessment of the nonlinear behaviour of rc structures subjected to seismic action: Smart 2013 shaking table test simulation. Engineering Structures, 759-773.

M. Berveiller, Y. Le Pape, B. Sudret and F. Perrin. (2012). Updating the long-term creep strains in concrete containment vessels by using markov chain monte carlo simulation and polynomial chaos expansion. Structure and Infrastructure Engineering, 425-440.

M. Berveiller, B. Sudret and M. Lemaire. (2006). Stochastic finite element: a non intrusive approach by regression. European Journal of Computational Mechanics, 81-92.

G. Blatman and B. Sudret. (2010). Efficient computation of global sensitivity indices using sparse polynomial chaos expansions. Reliability Engineering & System Safety, 1216-1229.

G. Blatman and B. Sudret. (2011). Adaptive sparse polynomial chaos expansion based on least angle regression. Journal of Computational Physics, 2345-2367.

Cast3M. (2019). Code de Calcule aux Eléments Finis CAST3M. Technical Report Commissariat à l'Energie Atomique, CEA-DES/DM2S/SEMT.

CEA, T. A. (2013). http://data-tamaris.fr/.

Hastings, W. (1970). Monte carlo sampling methods using markov chains and their applications. SCOPUS, 97-109.

Marelli, S. L. (2022). Technical Report Chair of Risk, Safety and Uncertainty Quantification, ETH Zurich, Switzerland. UQLab user manual – Polynomial chaos expansions.

METIS, S. r. (2020). https://metis-h2020.eu/.

Metropolis, N. R. (2004). Equation of State Calculations by Fast Computing Machines. The Journal of Chemical, 1087-1092.

B. Richard, L. Adelaide, C. Cremona, A. Orcesi. (2012). A methodology for robust updating of nonlinear structural models. Engineering Structures, 356-372.

B. Richard, S. Cherubini, F. Voldoire, P.-E. Charbonnel, T. Chaudat, S. Abouri, N. Bonfils. (2016). Smart 2013: Experimental and numerical assessment of the dynamic behavior by shaking table tests of an asymmetrical reinforced concrete structure subjected to high intensity ground motions. Engineering Structures, 99-116.

B. Richard, P. Martinelli, F. Voldoire, M. Corus, T. Chaudat, S. Abouri, N. Bonfils. (2015). Smart 2008: Shaking table tests on an asymmetrical reinforced concrete structure and seismic margins assessment. Engineering Structures, 48-61.

D. Rossat, D. E.-M. Bouhjiti, J. Baroth, M. Briffaut, F. Dufour, A. Monteil, B. Masson, S. Michel-Ponnelle. (2021). A bayesian strategy for forecasting the leakage rate of concrete containment buildings – application to nuclear containment buildings. Nuclear Engineering and Design, 111184.

D. Rossat, J. Baroth, M. Briffaut, F. Dufour, B. Masson, A. Monteil, S. Michel-Ponnelle. (2022). Bayesian updating for nuclear containment buildings using both mechanical and hydraulic monitoring data. Engineering Structures, 114294.

G. G. Tekeste, A. A. Correia and A. G. Costa. (2022). Bayesian updating of seismic fragility curves through experimental tests. Bulletin of Earthquake Engineering.

Z. Wang, I. Zentner, E. Zio. (2018). A Bayesian framework for estimating fragility curves based on seismic damage data and numerical simulations by adaptive neural networks. Nuclear Engineering and, 232-246.

11. Appendix

11.1. Detailed example for PCE application

In this appendix, the construction of the metamodel through the PCE approach is illustrated with two examples:

- case of the spectral acceleration ($S_a = \mathcal{M}(\xi_1 ; \xi_2)$) as a function of the two damping ratios ξ_1 and ξ_2 for a calibrated Young's modulus values (posterior values);
- case of the inter-storey drift ($\delta = \mathcal{M}(\xi_1 ; \xi_2)$) as a function of the two damping ratios ξ_1 and ξ_2 for a calibrated Young's modulus values (posterior values);

The development of the metamodels and Bayesian updating as well are done using Matlab and adapted open-source packages from UQLab (Marelli, 2022).

11.1.1. Metamodel for acceleration response spectra (run 9)

- Step 1: random values of the input parameters

Figure 38 illustrates an example of random values of damping ratios (ξ_1 ; ξ_2). Those values are extracted from the supposed distribution (section 6.1.2.1).

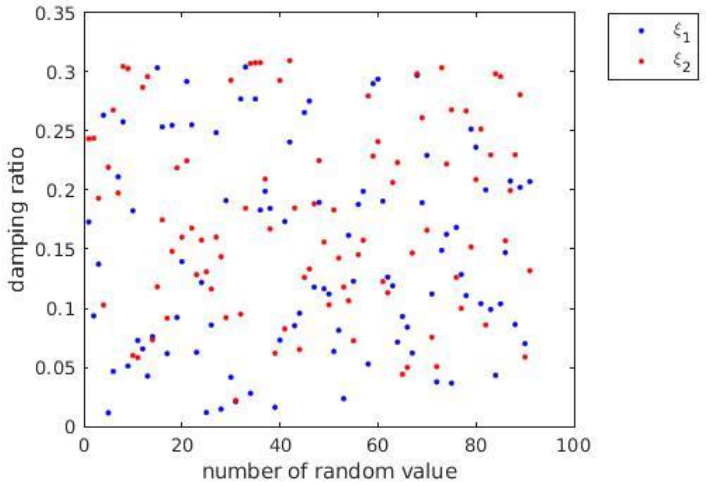

Figure 38: random values of damping ratios

- Step 2: output from finite element simulations

The numerical simulations are launched with different random values (100 values in Figure 38). Figure 39 presents the results of acceleration response spectra at the control point D.

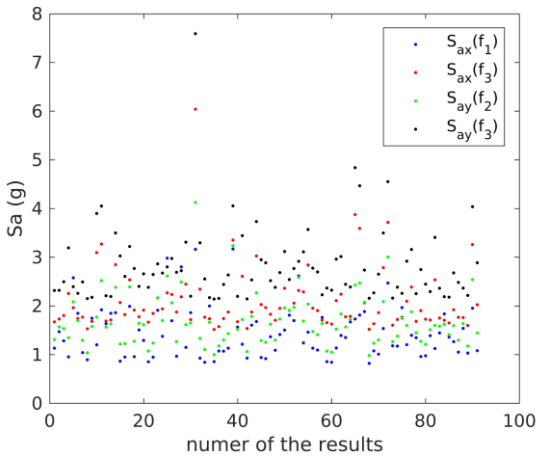

Figure 39: output as acceleration response spectra

- Step 3: Matlab toolbox

The input and output presented respectively in steps 1 and 2 are imported into our toolbox to compute the coefficients of polynomial based regression approach. The form of the polynomial function is dependent on the choice of the supposed distribution (here we consider the uniform distribution) as mentioned in Table 16.

Table 1: List of classical univariate polynomial families common in polynomial chaos expansion applications.

Type of variable	Distribution	Orthogonal polynomials	Hilbertian basis $\psi_k(x)$
Uniform	$\mathbf{1}_{]-1,1[}(x)/2$	Legendre $P_k(x)$	$P_k(x)/\sqrt{\frac{1}{2k+1}}$
Gaussian	$\frac{1}{\sqrt{2\pi}}e^{-x^2/2}$	Hermite $H_{e_k}(x)$	$H_{e_k}(x)/\sqrt{k!}$
Gamma	$x^a\, e^{-x}\, \mathbf{1}_{\mathbb{R}^+}(x)$	Laguerre $L_k^a(x)$	$L_k^a(x)/\sqrt{\frac{\Gamma(k+a+1)}{k!}}$
Beta	$\mathbf{1}_{]-1,1[}(x)\, \frac{(1-x)^a(1+x)^b}{B(a)\,B(b)}$	Jacobi $J_k^{a,b}(x)$	$J_k^{a,b}(x)/\mathfrak{J}_{a,b,k}$
		$\mathfrak{J}^2_{a,b,k} = \frac{2^{a+b+1}}{2k+a+b+1}\frac{\Gamma(k+a+1)\Gamma(k+b+1)}{\Gamma(k+a+b+1)\Gamma(k+1)}$	

Table 16: illustration the form of polynomials (Marelli, 2022)

The computed polynomial terms are presented in Table 17 with i and k are respectively the degree of polynomial term related to the damping ratios (ξ_1 ; ξ_2) and Y_{ik} the corresponding coefficients:

$$S_a \approx \sum_{i+k\leq 8} Y_{ik}\ \xi_1^i\ \xi_2^k$$

S_{ax} (f_1)		
i	k	Y_{ik}
0	0	0
0	1	-0.0919
1	0	-0.4627
0	2	0.00723
2	0	0.17197
1	1	0.0693
0	3	0
3	0	-0.0724
1	2	-0.0068
2	1	-0.0402
0	4	0
4	0	0.02654
2	2	0.00477
1	3	0
3	1	0.02198
0	5	0
5	0	-0.0127
2	3	-0.0009
3	2	-0.0039
1	4	0
4	1	-0.0112
0	6	0
6	0	0.01052
3	3	0.00086
2	4	0
4	2	0.00277
1	5	0
5	1	0.00889
0	7	0
7	0	-0.0074
3	4	0
4	3	0
2	5	0
5	2	0
1	6	0
6	1	-0.0075
0	8	0
8	0	0.00276

S_{ax} (f_3)		
i	k	Y_{ik}
0	0	0
0	1	-0.7434
1	0	-0.1627
0	2	0.39457
2	0	0.01467
1	1	0.14143
0	3	-0.1771
3	0	-0.0124
1	2	-0.1476
2	1	0.00175
0	4	0.05219
4	0	0.00915
2	2	-0.0013
1	3	0.1118
3	1	0
0	5	0
5	0	0
2	3	-0.0118
3	2	0
1	4	-0.0735
4	1	-0.008
0	6	-0.0027
6	0	0
3	3	0.00191
2	4	0.00877
4	2	0.00794
1	5	0.03225
5	1	0
0	7	0
7	0	0.00111

S_{ay} (f_2)		
i	k	Y_{ik}
0	0	0
0	1	-0.3069
1	0	-0.3698
0	2	0.06622
2	0	0.11788
1	1	0.10073
0	3	-0.0186
3	0	-0.0157
1	2	-0.0125
2	1	-0.0965
0	4	0
4	0	0
2	2	0.06133
1	3	0
3	1	0.00787
0	5	0
5	0	0
2	3	-0.0455
3	2	0
1	4	0
4	1	0
0	6	0
6	0	0
3	3	0
2	4	0.02431
4	2	0
1	5	0
5	1	0
0	7	0
7	0	0

S_{ay} (f_3)		
i	k	Y_{ik}
0	0	0
0	1	-1.1032
1	0	-0.016
0	2	0.66833
2	0	0.01558
1	1	0.03829
0	3	-0.415
3	0	-0.0056
1	2	-0.0535
2	1	-0.0214
0	4	0.23341
4	0	0
2	2	0.02287
1	3	0.04263
3	1	0.00781
0	5	-0.118
5	0	0
2	3	-0.0117
3	2	-0.0017
1	4	-0.0193
4	1	-0.0041
0	6	0.03894
6	0	0

Table 17: coefficients of polynomial function (spectral acceleration #run9)

The comparison of the estimation of metamodel with numerical simulation is found in Figure 27.

11.1.2. Metamodel for inter-storey drift (run 9)

- Step 1: random values of input parameters

Metamodel for inter-storey drift shares the same input random values (ξ_1 ; ξ_2) as illustrated in Figure 38.

- Step 2: output from finite element simulations

The output interest of the simulations are the inter-storey drift at point D (Figure 40).

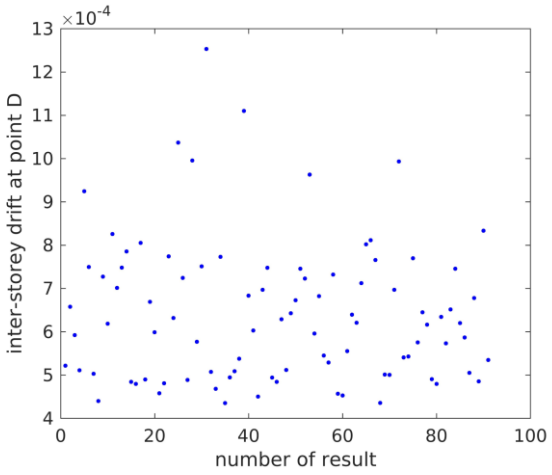

Figure 40: output as inter-storey drift at point D

- Step 3: Matlab toolbox

The same strategy is followed as in the previous case:

$$\delta \approx \sum_{i+k\leq 7} Y_{ik}\ \xi_1^i\ \xi_2^k$$

The coefficients of the polynomial function are presented in

Drift at point D		
i	k	Y_{ik}
0	0	0
0	1	-5.79E-05
1	0	-0.0001394
0	2	1.82E-05
2	0	4.26E-05
1	1	2.10E-05
0	3	-8.86E-06

continue		
i	k	Y_{ik}
0	5	0
5	0	-2.56E-06
2	3	-9.11E-08
3	2	0
1	4	-5.49E-06
4	1	-1.73E-06
0	6	-1.95E-07

3	0	-1.24E-05	6	0	2.21E-06
1	2	-9.89E-06	3	3	0
2	1	-7.36E-06	2	4	2.45E-07
0	4	2.89E-06	4	2	-1.59E-06
4	0	3.99E-06	1	5	1.38E-06
2	2	-9.91E-07	5	1	1.12E-06
1	3	8.34E-06	0	7	0
3	1	9.34E-06	7	0	0

Table 18 and the comparison of metamodel is shown in Figure 41.

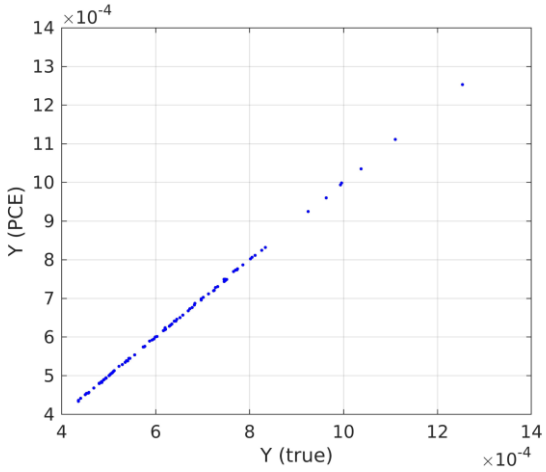

Figure 41: comparison of metamodel response vs. computed values using Cast3m

Drift at point D		
i	k	Y_{ik}
0	0	0
0	1	-5.79E-05
1	0	-0.0001394
0	2	1.82E-05
2	0	4.26E-05
1	1	2.10E-05
0	3	-8.86E-06
3	0	-1.24E-05
1	2	-9.89E-06
2	1	-7.36E-06
0	4	2.89E-06
4	0	3.99E-06
2	2	-9.91E-07
1	3	8.34E-06
3	1	9.34E-06

continue		
i	k	Y_{ik}
0	5	0
5	0	-2.56E-06
2	3	-9.11E-08
3	2	0
1	4	-5.49E-06
4	1	-1.73E-06
0	6	-1.95E-07
6	0	2.21E-06
3	3	0
2	4	2.45E-07
4	2	-1.59E-06
1	5	1.38E-06
5	1	1.12E-06
0	7	0
7	0	0

Table 18: coefficients of polynomial function (drift #run9)

11.2. Run #9

11.2.1. Metamodel for the 2nd Bayesian (ξ_1; ξ_2 ➔ S_a)

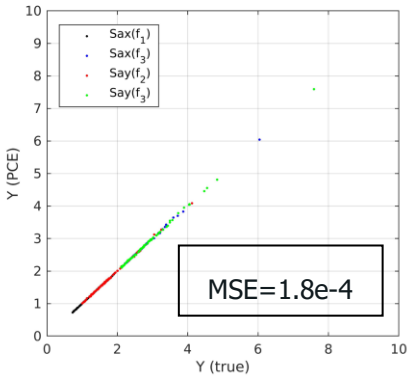

Figure 42: comparison of Metamodel with numerical simulation (run #9)

11.2.2. Updated damping ratios

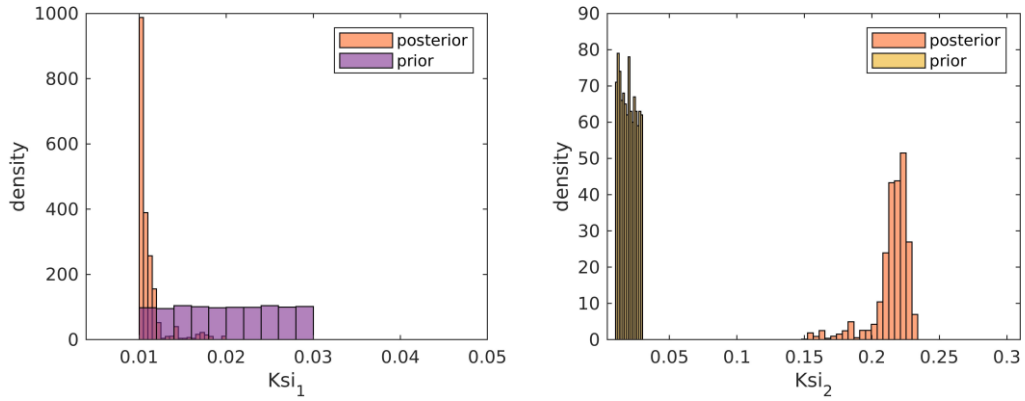

Figure 43: prior/posterior damping ratios distribution

11.2.3. Verification

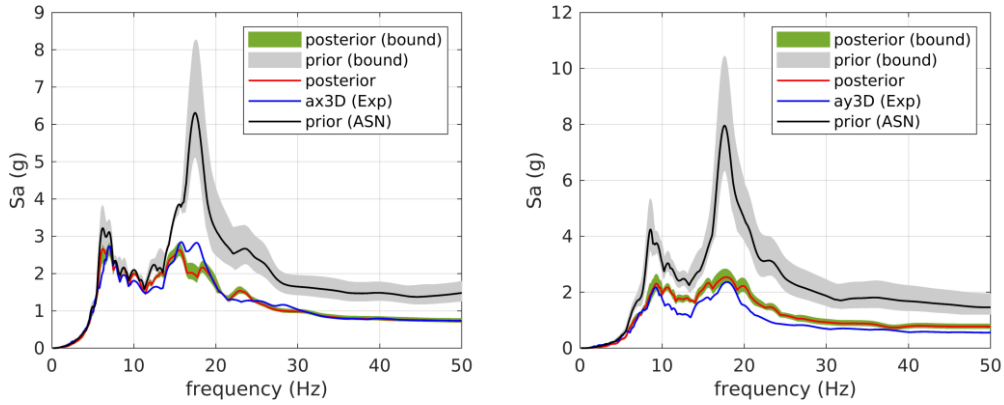

Figure 44: comparison of acceleration response spectra (5%) at point D

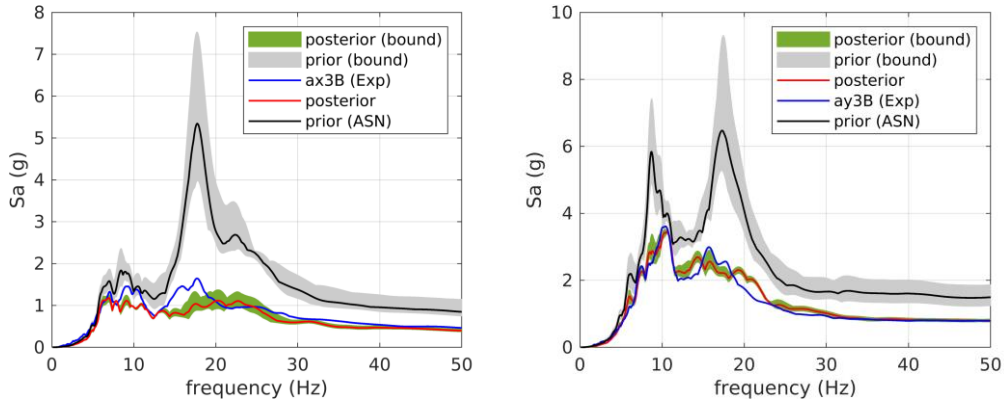

Figure 45: comparison of acceleration response spectra (5%) at point B

11.3. Run #11

11.3.1. Metamodel for the 2nd Bayesian (ξ_1; ξ_2 ➔ S_a)

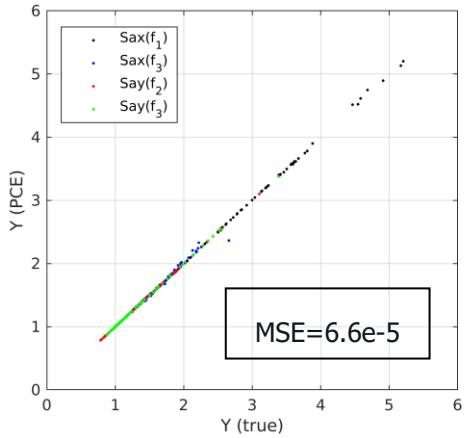

Figure 46: comparison of Metamodel with numerical simulation (run #11)

11.3.2. Updated damping ratios

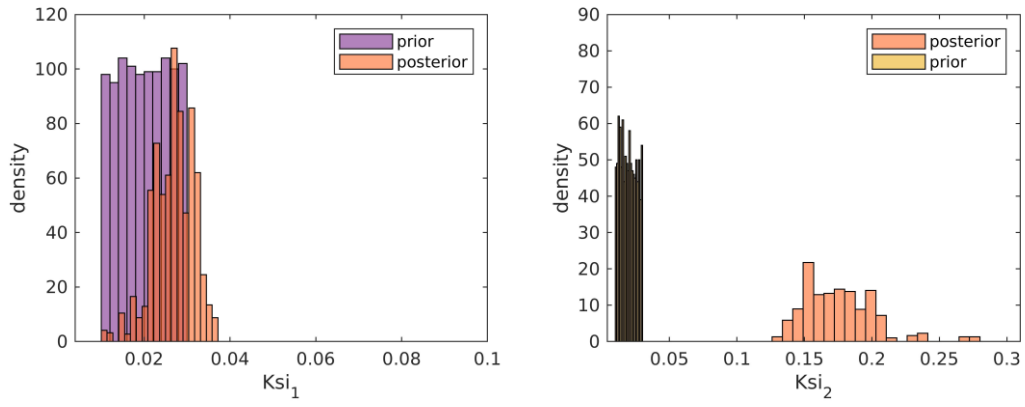

Figure 47: prior/posterior damping ratios distribution

11.3.3. Verification

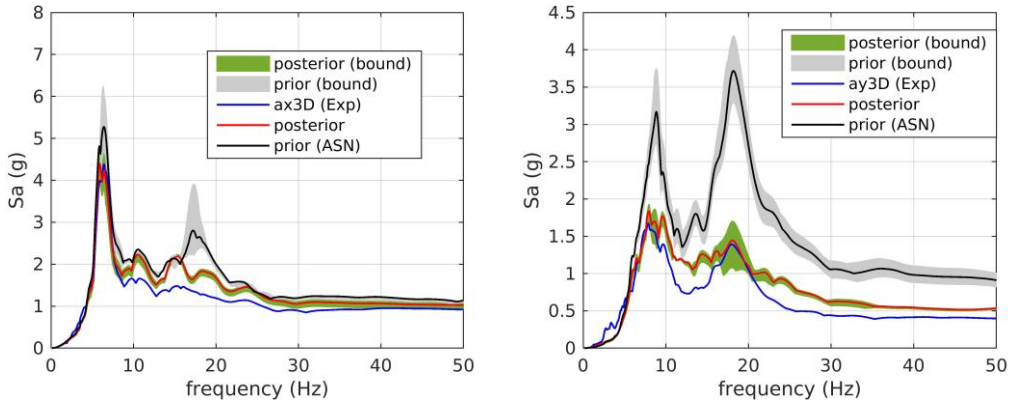

Figure 48: comparison of acceleration response spectra (5%) at point D

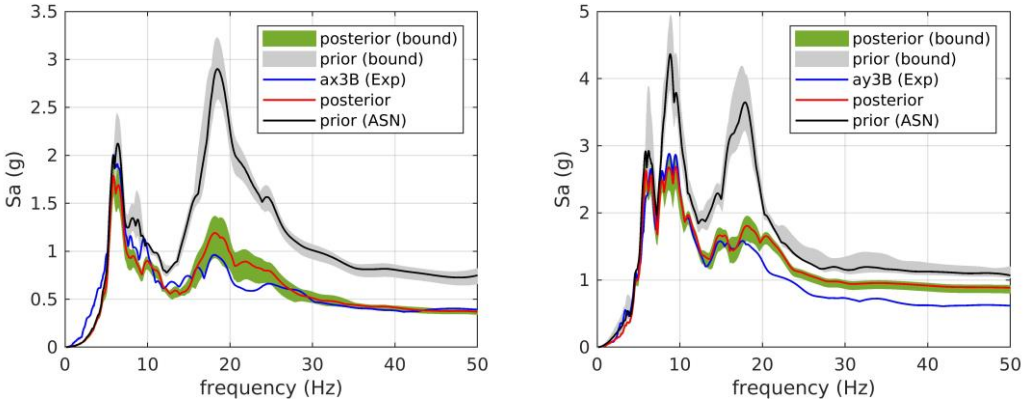

Figure 49: comparison of acceleration response spectra (5%) at point B

11.4. Run #15

11.4.1. Updated Young's modulus

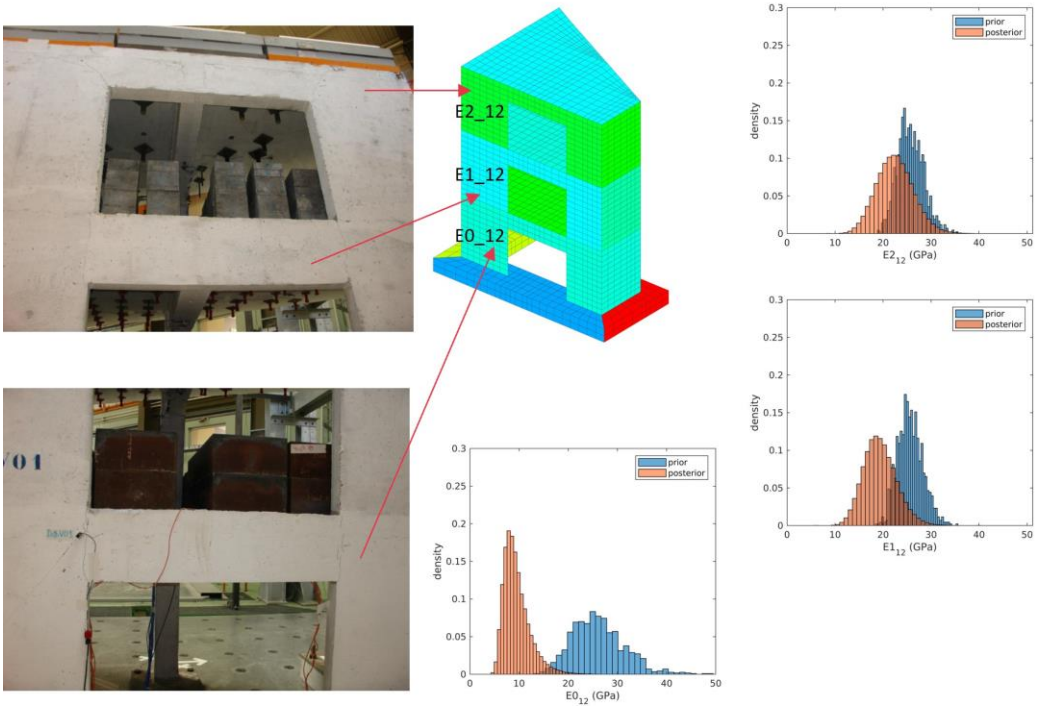

Figure 50: prior/posterior Young's modulus distribution (wall : V_{12})

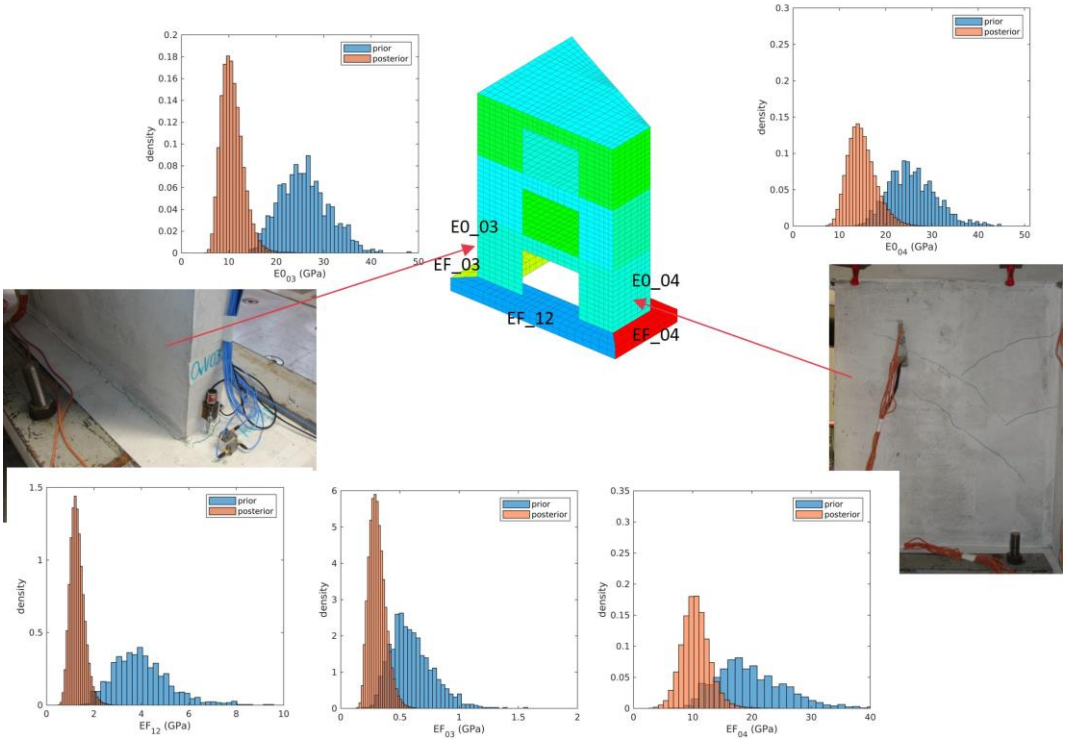

Figure 51: prior/posterior Young's modulus distribution (wall + foundation)

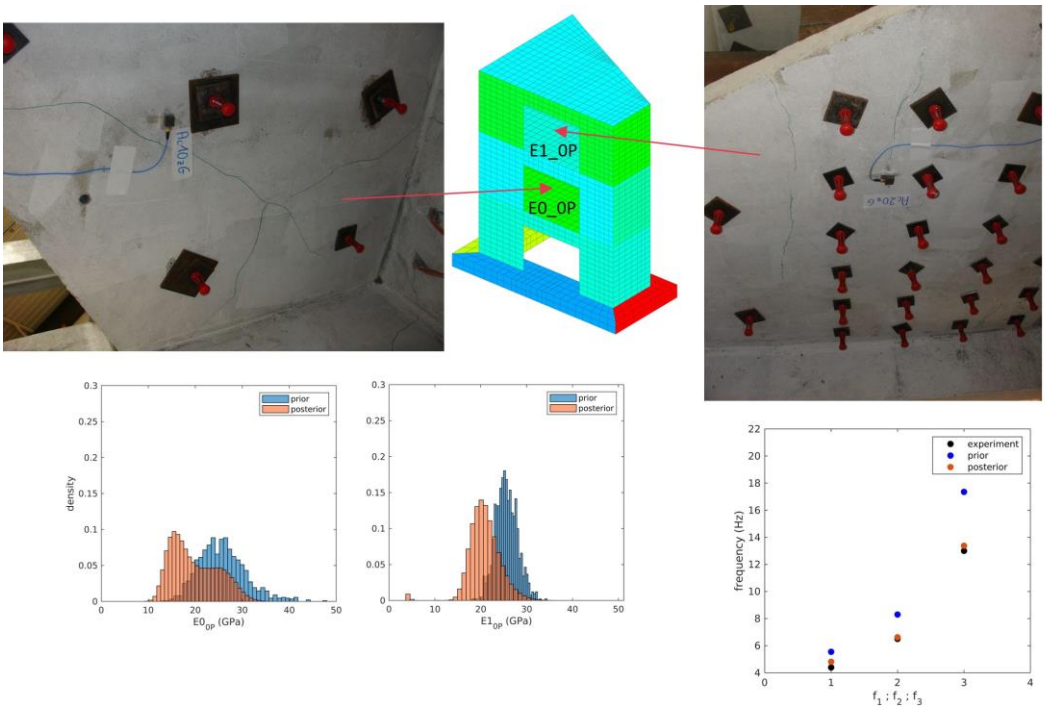

Figure 52: prior/posterior Young's modulus distribution (slab)

Prior/posterior: (MCMC=1e5 chains; 100 values/chain	remarque
$E0_{12}$: (μ = 25700 MPa / 9500 MPa ; Cov = 20%/28%)	-
$E0_{03}$: (μ = 25700 MPa / 11000 MPa ; Cov = 20%/22%)	-
$E0_{04}$: (μ = 25700 MPa / 15000 MPa ; Cov = 20%/20%)	-
$E0_{P}$: (μ = 25700 MPa / 19800 MPa ; Cov = 20%/25%)	-
$E1_{12}$: (μ = 25700 MPa / 20000 MPa ; Cov = 20%/17%)	-
$E1_{03}$: 25700 MPa (constant)	No crack
$E1_{04}$: 25700 MPa (constant)	No crack
$E1_{P}$: (μ = 25700 MPa / 21000 MPa ; Cov = 10%/16%)	-
$E2_{12}$: (μ = 25700 MPa / 22500 MPa ; Cov = 10%/17%)	-
$E2_{03}$: 25700 MPa (constant)	No crack
$E2_{04}$: 25700 MPa (constant)	No crack
$E2_{P}$: 25700 MPa (constant)	No crack
E_{F12} : (μ = 4000 MPa / 1300 MPa ; Cov = 20%/23%)	-
E_{F03} : (μ = 600 MPa / 310 MPa ; Cov = 20%/22%)	-
E_{F04} : (μ = 20000 MPa / 10500 MPa ; Cov = 20%/22%)	-

Table 19: prior and posterior of Young's modulus

11.4.2. Metamodel for the 2nd Bayesian (ξ_1; ξ_2 ➔ S_a)

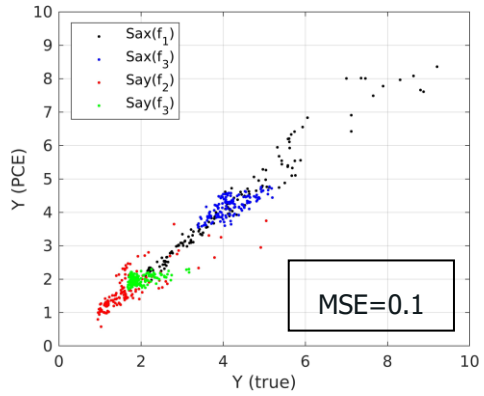

Figure 53: comparison of Metamodel with numerical simulation (run #15)

11.4.3. Updated damping ratios

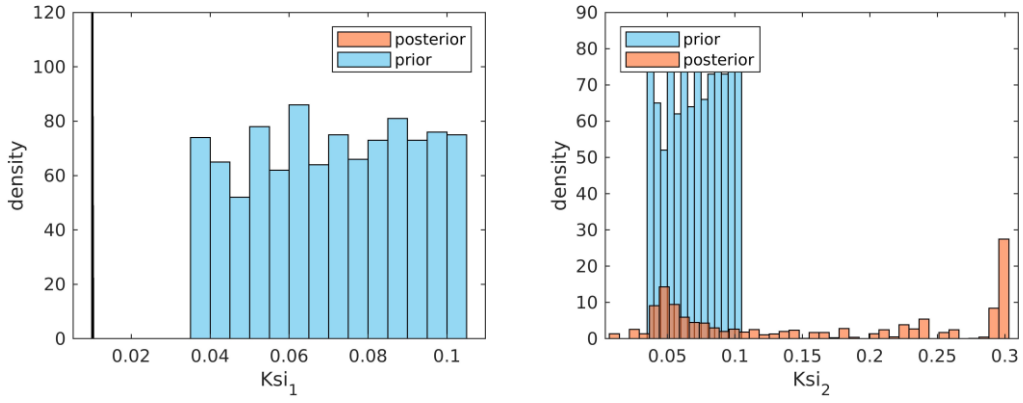

Figure 54: prior/posterior damping ratios distribution

11.4.4. Verification

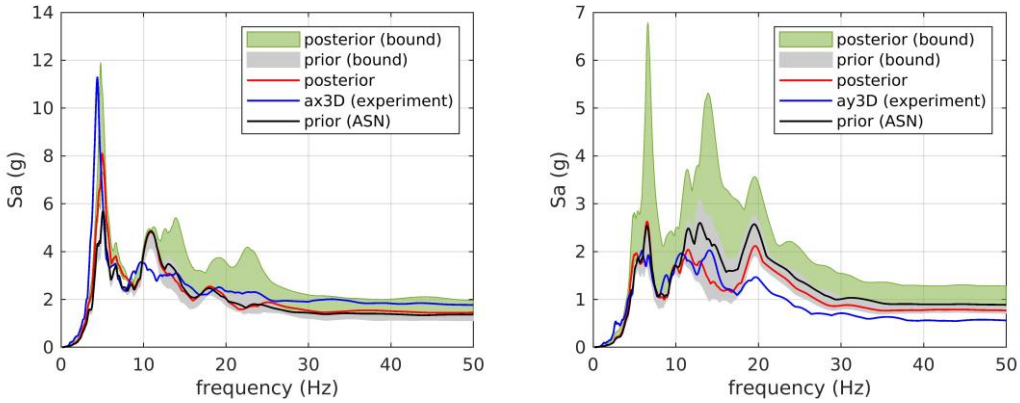

Figure 55: comparison of acceleration response spectra (5%) at point D

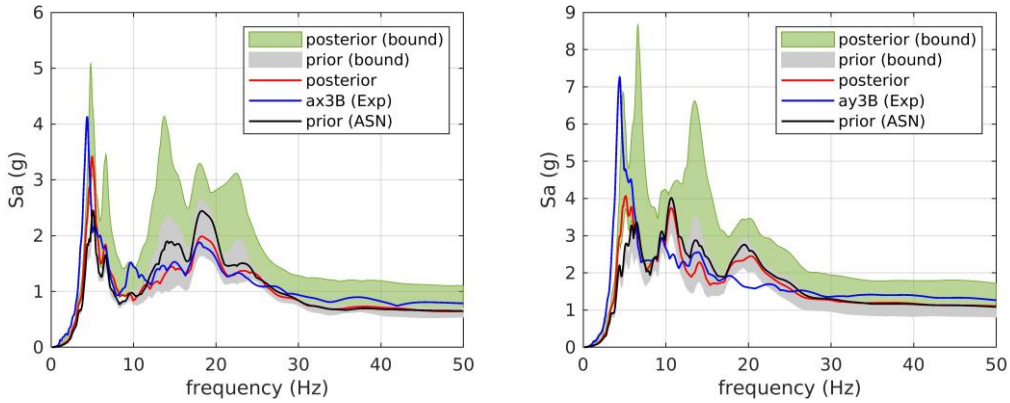

Figure 56: comparison of acceleration response spectra (5%) at point B

11.5. Run #17

11.5.1. Updated Young's modulus

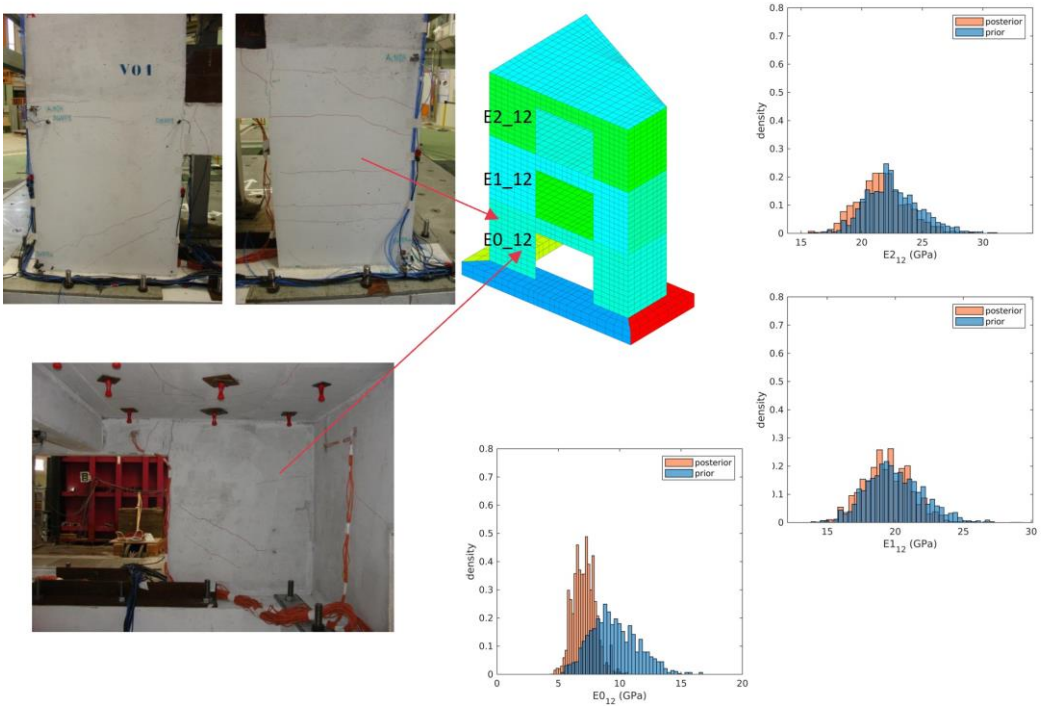

Figure 57: prior/posterior Young's modulus distribution (wall : V_{12})

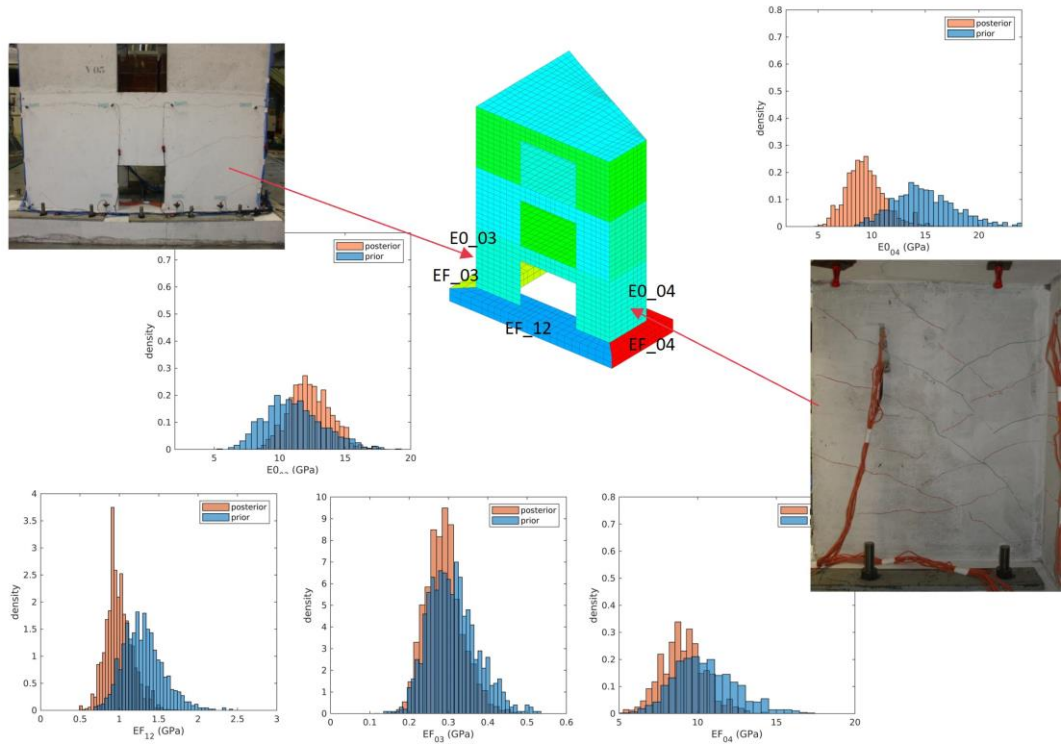

Figure 58: prior/posterior Young's modulus distribution (wall + foundation)

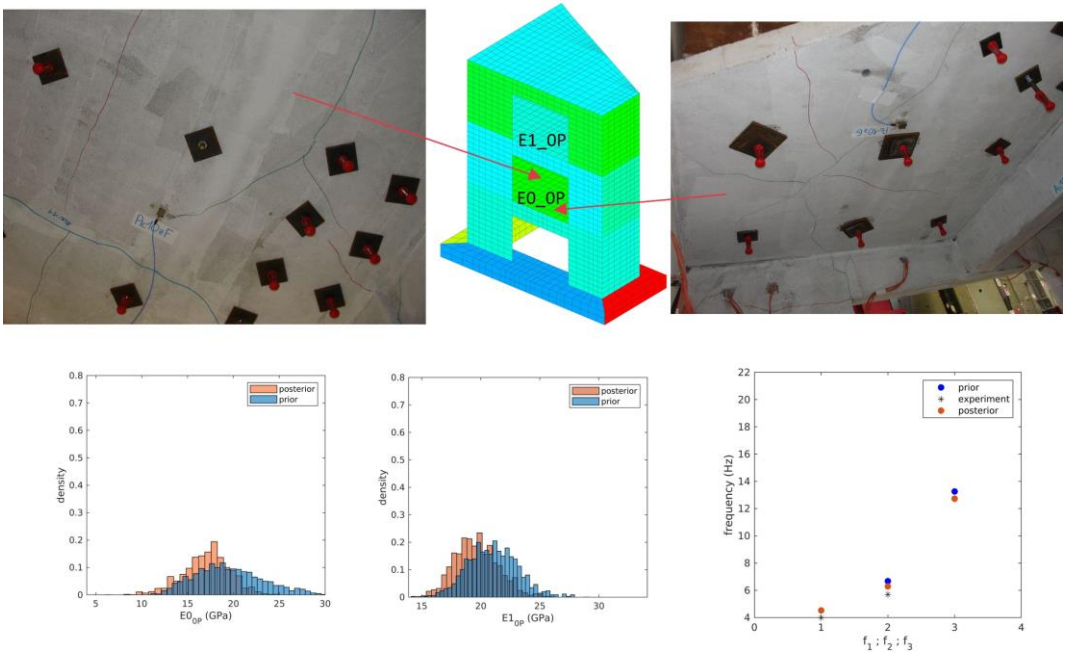

Figure 59: prior/posterior Young's modulus distribution (slab)

Prior/posterior: (MCMC=1e5 chains; 100 values/chain	remarque
$E0_{12}$: (μ = 9500 MPa / 7200 MPa ; Cov = 20%/13%)	-
$E0_{03}$: (μ = 11000 MPa / 12000 MPa ; Cov = 20%/13%)	-
$E0_{04}$: (μ = 15000 MPa / 9400 MPa ; Cov = 20%/19%)	-
$E0_{P}$: (μ = 19800 MPa / 17000 MPa ; Cov = 20%/15%)	-
$E1_{12}$: (μ = 20000 MPa / 19400 MPa ; Cov = 10%/9%)	-
$E1_{03}$: 25700 MPa (constant)	No crack
$E1_{04}$: 25700 MPa (constant)	No crack
$E1_{P}$: (μ = 21000 MPa / 19600 MPa ; Cov = 10%/9%)	-
$E2_{12}$: (μ = 22500 MPa / 21000 MPa ; Cov = 10%/9%)	-
$E2_{03}$: 25700 MPa (constant)	No crack
$E2_{04}$: 25700 MPa (constant)	No crack
$E2_{P}$: 25700 MPa (constant)	No crack
E_{F12} : (μ = 1300 MPa / 1000 MPa ; Cov = 20%/17%)	-
E_{F03} : (μ = 310 MPa / 288 MPa ; Cov = 20%/16%)	-
E_{F04} : (μ = 10500 MPa / 9000 MPa ; Cov = 20%/15%)	-

Table 20: prior and posterior of Young's modulus

11.5.2. Metamodel for the 2nd Bayesian (ξ_1; ξ_2 ➔ S_a)

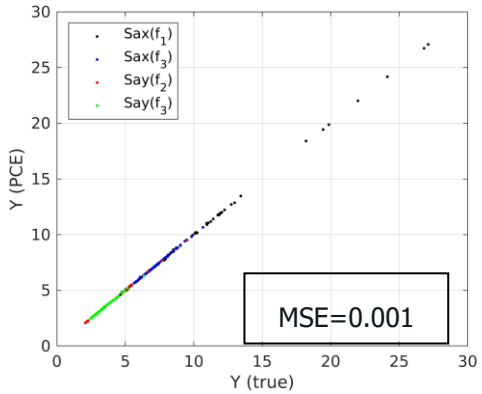

Figure 60: comparison of Metamodel with numerical simulation (run #17)

11.5.3. Updated damping ratios

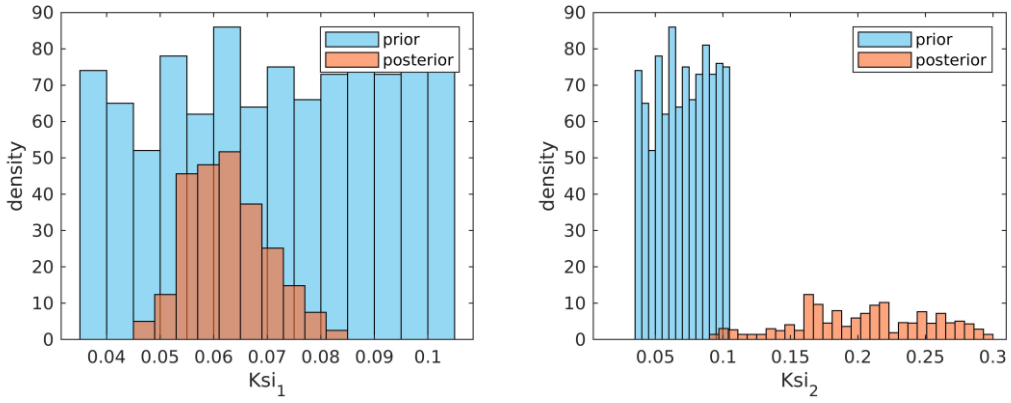

Figure 61: prior/posterior damping ratios distribution

11.5.4. Verification

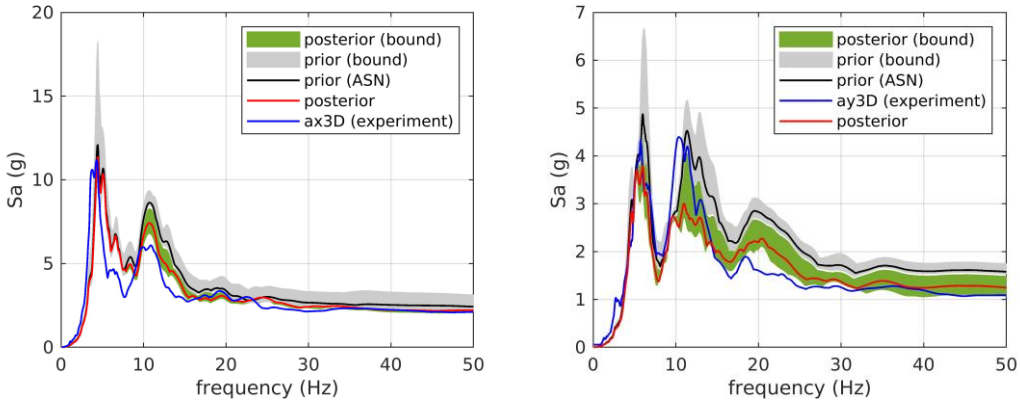

Figure 62: comparison of acceleration response spectra (5%) at point D

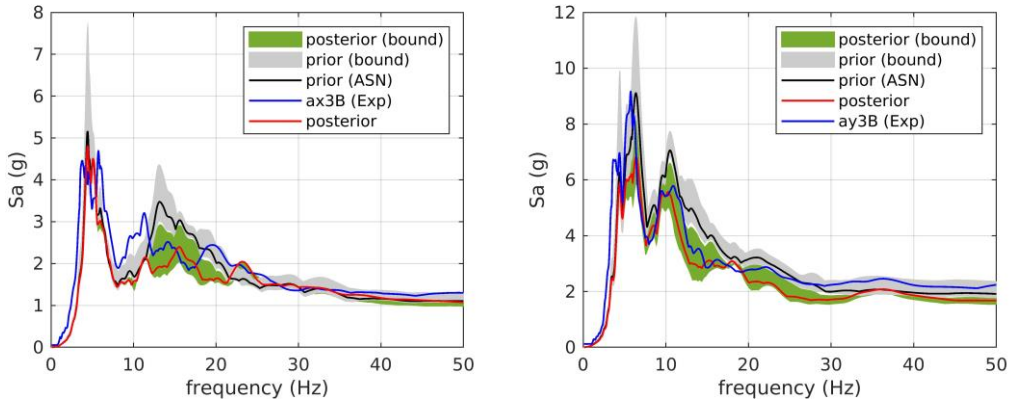

Figure 63: comparison of acceleration response spectra (5%) at point B